ISSN 2150-5330 (online)

World Journal of *Gastrointestinal Pathophysiology*

World J Gastrointest Pathophysiol 2020 June 20; 11(4): 78-103

Published by Baishideng Publishing Group Inc

WJGP

World Journal of Gastrointestinal Pathophysiology

Contents

Irregular Volume 11 Number 4 June 20, 2020

MINIREVIEWS

ORIGINAL ARTICLE

Basic Study

Contents

World Journal of Gastrointestinal Pathophysiology

Volume 11 Number 4 June 20, 2020

ABOUT COVER

Editorial Board Member of *World Journal of Gastrointestinal Pathophysiology*, Bhornprom Yoysungnoen, PhD, Associate Professor, Senior Lecturer, Division of Physiology, Faculty of Medicine, Thammasat University, Pathumthani 12120, Thailand

AIMS AND SCOPE

The primary aim of the *World Journal of Gastrointestinal Pathophysiology* (*WJGP*, *World J Gastrointest Pathophysiol*) is to provide scholars and readers from various fields of gastrointestinal pathophysiology with a platform to publish high-quality basic and clinical research articles and communicate their research findings online.

WJGP mainly publishes articles reporting research results and findings obtained in the field of gastrointestinal pathophysiology and covering a wide range of topics including disorders of the esophagus, stomach and duodenum, small intestines, pancreas, biliary system, and liver.

INDEXING/ABSTRACTING

The *WJGP* is now abstracted and indexed in Emerging Sources Citation Index (Web of Science), PubMed, PubMed Central, China National Knowledge Infrastructure (CNKI), and Superstar Journals Database.

RESPONSIBLE EDITORS FOR THIS ISSUE

Responsible Electronic Editor: *Lu-Lu Qi*

Proofing Production Department Director: *Xiang Li*

Responsible Editorial Office Director: *Jia-Ping Yan*

NAME OF JOURNAL
World Journal of Gastrointestinal Pathophysiology

ISSN
ISSN 2150-5330 (online)

LAUNCH DATE
April 15, 2010

FREQUENCY
Irregular

EDITORS-IN-CHIEF
Somchai Amornyotin, Kusum K Kharbanda, Tsutomu Nishida

EDITORIAL BOARD MEMBERS
https://www.wjgnet.com/2150-5330/editorialboard.htm

PUBLICATION DATE
June 20, 2020

INSTRUCTIONS TO AUTHORS
https://www.wjgnet.com/bpg/gerinfo/204

GUIDELINES FOR ETHICS DOCUMENTS
https://www.wjgnet.com/bpg/GerInfo/287

GUIDELINES FOR NON-NATIVE SPEAKERS OF ENGLISH
https://www.wjgnet.com/bpg/gerinfo/240

PUBLICATION ETHICS
https://www.wjgnet.com/bpg/GerInfo/288

PUBLICATION MISCONDUCT
https://www.wjgnet.com/bpg/gerinfo/208

ARTICLE PROCESSING CHARGE
https://www.wjgnet.com/bpg/gerinfo/242

STEPS FOR SUBMITTING MANUSCRIPTS
https://www.wjgnet.com/bpg/GerInfo/239

ONLINE SUBMISSION
https://www.f6publishing.com

World Journal of Gastrointestinal Pathophysiology

Submit a Manuscript: https://www.f6publishing.com

World J Gastrointest Pathophysiol 2020 June 20; 11(4): 78-83

DOI: 10.4291/wjgp.v11.i4.78

ISSN 2150-5330 (online)

MINIREVIEWS

Correlations of morphology and molecular alterations in traditional serrated adenoma

Hongxing Gui, Michael A Husson, Rifat Mannan

ORCID number: Hongxing Gui (0000-0002-9686-6006); Michael A Husson (0000-0001-9898-3815); Rifat Mannan (0000-0003-1735-7770).

Author contributions: Gui H collected, analyzed the data and drafted the manuscript; Husson MA and Mannan R critically revised and finally approved the manuscript.

Conflict-of-interest statement: There is no conflict of interest.

Manuscript source: Unsolicited manuscript

Received: January 10, 2020
Peer-review started: January 10, 2020
First decision: January 28, 2020
Revised: March 27, 2020
Accepted: May 27, 2020
Article in press: May 27, 2020
Published online: June 20, 2020

P-Reviewer: Aoki H, Li WB

Hongxing Gui, Michael A Husson, Rifat Mannan, Department of Pathology and Laboratory Medicine, Pennsylvania Hospital of the University of Pennsylvania Health System, Philadelphia, PA 19107, United States

Corresponding author: Hongxing Gui, MD, PhD, Doctor, Department of Pathology and Laboratory Medicine, Pennsylvania Hospital of the University of Pennsylvania Health System, 801 Spruce Street, 10th Floor Spruce Building, Philadelphia, PA 19107, United States. hongxing.gui@uphs.upenn.edu

Abstract

Traditional serrated adenoma was first reported by Longacre and Fenoglio-Presier in 1990. Their initial study described main features of this lesion, but the consensus diagnostic criteria were not widely adopted until recently. Traditional serrated adenoma presents with grossly protuberant configuration and pinecone-like appearance upon endoscopy. Histologically, it is characterized by ectopic crypt formation, slit-like serration, eosinophilic cytoplasm and pencillate nuclei. Although much is now known about the morphology and molecular changes, the mechanisms underlying the morphological alterations are still not fully understood. Furthermore, the origin of traditional serrated adenoma is not completely known. We review recent studies of the traditional serrated adenoma and provide an overview on current understanding of this rare entity.

Key words: Traditional serrated adenoma; Serrated polyps; *KRAS*; *BRAF*; Colon

Core tip: This mini-review summarizes recent findings of traditional serrated adenoma. The origin of traditional serrated adenoma and its molecular pathogenesis are discussed in details.

Citation: Gui H, Husson MA, Mannan R. Correlations of morphology and molecular alterations in traditional serrated adenoma. *World J Gastrointest Pathophysiol* 2020; 11(4): 78-83
URL: https://www.wjgnet.com/2150-5330/full/v11/i4/78.htm
DOI: https://dx.doi.org/10.4291/wjgp.v11.i4.78

S-Editor: Wang JL
L-Editor: A
E-Editor: Wu YXJ

INTRODUCTION

Colorectal carcinoma (CRC) is a heterogeneous disease in terms of its molecular pathways of carcinogenesis. Most, if not all CRCs, arise from conventional adenomas or serrated lesions, the latter accounting for 5%-35% of CRC[1,2]. Serrated polyps include hyperplastic polyps (HPs), sessile serrated lesions (SSLs), traditional serrated adenomas (TSAs) and unclassified serrated adenomas according to 2019 World Health Organization classification of colonic epithelial neoplasms[3]. Sessile serrated lesions and TSAs are regarded as precursors to CRC, while small HPs are considered to have little risk for neoplastic progression. TSAs comprise 0.56%-1.9% of colorectal polyps and are the least characterized serrated lesions in the colorectal carcinogenesis[4-6]. Endoscopically, TSAs show exophytic protuberant configuration and pinecone-like appearance[7,8]. Histologically, TSAs feature architectures of complex filiform or villiform growth pattern, slit-like or flat-top serration and ectopic crypt formation (ECF) which is defined as small rudimental crypts located on the side of villous structure and displaced from bottom muscularis mucosa. Cytologically, TSA is characterized by lining of epithelium with abundant eosinophilic cytoplasm, pseudostratified pencillate nuclei and dispersed chromatin (Figure 1)[9]. Although it is debatable which feature is the most sensitive and which one is the most specific, it is agreed that none of them alone is sufficient or required for diagnosing TSA. Fulfilling 2 out of 3 core features (ECF, eosinophilic cytoplasm and slit-like serration) may be more reproducible in making the diagnosis of TSA[10].

The molecular pathogenesis of TSA is poorly understood due to its rarity. Less is known about the mechanism that drives precursor lesions and their subsequent risk of progression. In this review, we will present the currently available literature, focusing on the origin of TSA. We will also attempt to correlate the molecular changes with morphologic features, which might help us understand how TSAs develop from precursor lesions or *de novo*.

ORIGIN OF TSA

TSAs are probably underdiagnosed by pathologists for several reasons. TSAs are the rarest among the three serrated colonic polyps, comprising of about 5% serrated polyps and 0.56%-1.9% of all colorectal polyps[4-6], and widely accepted consensus criteria for diagnosing TSA were not available until recently. Chetty[11] listed a constellation of architectural and cytological features of TSA in a succinct review of the entity. However, none of these features are unique or specific for TSA. The minimal criteria for diagnosing TSA are also not specified in many studies. Additionally, TSAs are often admixed with HP or SSL[8,12,13], causing difficulty in recognition. Three variants of TSA were described, the prototypical filiform TSA, the less common flat TSA[12] and the rare mucin-rich TSA[9].

Genetic heterogeneity of TSAs contributes to the variation in cytomorphology. Almost 90% of TSAs develop through two mutually exclusive pathways: *BRAF* mutation (56.4%) and *KRAS* mutation (31.9%)[8,12-15] (Table 1). The remaining 10% may have other pathways involved such as EGFR (Figure 2)[16] that appears to segregate with *KRAS*-mutated polyps[12]. *BRAF* gene encodes an anti-apoptotic serine-threonine kinase. *BRAF* V600E activating mutation is an early event that drives serrated lesion into CRC[17,18]. TSAs with *BRAF* mutation often show a flat growth pattern with serrated dysplasia, high CpG island methylator phenotype (CIMP) and are more likely located in the proximal colon than *KRAS*-mutated TSA[8,12]. *KRAS*-mutated TSA are usually distally located and exophytic with adenomatous dysplasia. In addition to *KRAS* mutation, TSAs from distal colon show selective methylation of *SMOC1* gene and loss of its expression, which are also frequently associated with high-grade adenoma and CIMP-low/microsatellite stable CRC[19].

TSAs may arise from precursor lesions of microvesicular HP or SSL or may occur *de novo*. *BRAF* mutated TSAs are also more likely admixed or associated with HP or SSL-like lesions, which are identified in TSA in 38%-52.3% of cases[8,12,20]. One early study suggested that serrated precursor lesions adjacent to distal TSA are distinguished from SSL by lack of Annexin A10 despite shared morphologic and molecular features[21]. Annexin A10 is normally expressed in upper gastrointestinal tract[22]. It is identified as a marker of SSL[23] and is expressed in colorectal cancer of serrated pathway undergoing gastric programming[24]. Thus, it is not surprising that the serrated precursor lesions of TSA in this study, arising predominantly from distal colon, are distinctive from proximal colonic SSL[21]. It is more likely that small flat TSAs identified in proximal colon would be expressing Annexin A10. More recently, Bettington and colleagues compared small polyps (< 1 cm) (71% from the distal colon)

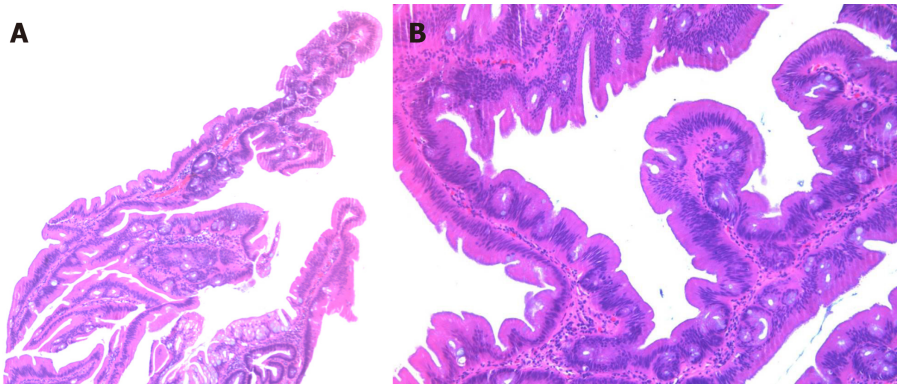

Figure 1 Low and high power view of the traditional serrated adenoma. A: A low power view (40×) of the traditional serrated adenoma shows viliform growth of the polyp with slit-like serration; B: A high power view (100×) demonstrates ectopic crypt formation, eosinophilic cytoplasm and pencillate nuclei.

and shoulder lesion in large TSAs, demonstrating similar immunophenotypic and molecular profiles[20]. These findings support that small TSAs do exist and may arise at least partially from some HP/SSL-like precursors.

WNT signaling is the main driver of colon cancer and physiological proliferation of colonic crypts[25]. Alterations in components of WNT pathway including mutations of *RNF43*, *APC* and *CTNNB1*, and overexpression of *RSPO* (due to fusion gene or amplification), can all lead to stabilization and nuclear localization of β-catenin and activation of WNT signaling[26]. Nuclear β-catenin staining, as well as p53 positivity, loss of p16 and *MLH1* promoter methylation is seen in the late development of polyps with dysplastic features[12,13]. However some molecular studies showed that components of WNT signaling are frequently altered in TSAs (30%-70%) regardless of the degree of dysplasia[15,27]. A recent study using microdissection to interrogate genetic changes revealed a stepwise molecular change in TSAs and associated precursors[28]. Clonally, the HP/SSL-like precursors share the identical mitogen-activated protein kinase (MAPK) pathway gene mutations (*BRAF* or *KRAS*) with TSAs. However, these precursors exhibit fewer mutated *WNT* pathway genes or heterozygotic mutations (*i.e.*, *RNF43*, *APC*, and *CTNNB1*) than TSA with biallelic inactivation. This study supports the sequence of MAPK to WNT alterations in TSA developing from HP and SSL-like lesions (Figure 2). One drawback of this study is that only one out of 15 polyps had *KRAS* mutation. Hence TSAs with *KRAS* mutation, which are predominantly found in the distal colon and typically are large in size, remain of uncertain in terms of origin and critical molecular alterations during development.

HISTOLOGIC-MOLECULAR CORRELATIONS

The presence of histologic features in TSAs is highly variable depending on their size and location. ECF is considered relatively more specific whereas slit-like serration and typical cytology are more sensitive features (Table 1). Serration is the common feature of HP, SSL and TSA. However, the cytomorphology of these three entities differs, reflecting distinct mechanisms underlying their development. *BRAF* or *KRAS* are two initiating mutations commonly seen in serrated polyps, activating MAPK pathway. HPs are characterized by saw-toothed serration in the upper half to third of the crypts and absence of basal crypt dilation[29,30]. Epithelial proliferation with defective apoptosis[5], delayed crypt cellular migration and maturation toward the surface leads to infolding of epithelial lining and formation of HPs. The majority of HPs are innocuous, largely because *KRAS* mutation in HP does not expand the stem cell pool but instead increases transit-amplifying cells in the mid and upper regions of crypts[31].

By contrast, SSLs have irregular proliferative zones and bidirectional maturation toward both surface and base of the crypt, causing pathognomonic basal crypt dilation and lateral spread of crypt base[32]. This architectural change was suggested to be similar to gastric foveolar growth pattern characterized by a mid-level proliferative compartment and bidirectional differentiation[11]. Another salient feature of SSLs is prominent inhibition of apoptosis in contrast to HPs and TSAs[33].

Compared to HP and SSL, TSAs have slit-like, flat-top serration rather than saw-toothed serration. Eosinophilic cells in TSA with luminal brush border and a

Table 1 Histologic and molecular changes in traditional serrated adenoma

Country/Territory	Polyp	Distal	*BRAF*	*KRAS*	Wild type	ECF	Slit-like serration	Typical cytology	Ref.
United States	24	96% (23)	29% (7)	46% (11)	25% (6)	NA	NA	79% (19)	[14]
South Korea	107	74.8% (80)	55.1% (59)	33.6% (36)	11.2% (12)	79.4% (85)	100% (107)	100% (107)	[8]
Taiwan	60	61.7% (37)	35% (21)	52% (31)	13.3% (8)	NA	NA	NA	[13]
Australia	200	71% (142)	67% (134)	22% (43)	11% (23)	89% (178)	98% (196)	100% (200)	[12]
Japan	129	82.2% (106)	61.2% (79)	34.8% (45)	3.9% (5)	NA	NA	NA	[15]
Australia	70	71% (50)	47% (33)	31% (22)	21% (15)	67% (47)	81% (57)	NA	[20]
Total	590	74.2% (438)	56.4% (333)	31.9%(188)	11.7% (69)	82% (310/377)	95% (360/377)	98.5% (326/331)	

Numbers in parenthesis are case numbers. ECF: Ectopic crypt formation; NA: Not applicable.

prominent villiform growth pattern are the features reminiscent of small intestine morphology[9]. It was believed that eosinophilic cytoplasm seen in TSA is due to cellular senescence[32]. Senescence and apoptosis are two protecting approaches of cells and tissue in response to oncogenic stresses[34]. They are the barriers that must be overcome in precursor lesions to promote and progress into fully developed TSAs. In TSAs, depending on locations, *BRAF* or *KRAS* are the initiating mutations activating MAPK pathway. Both, however, may cause cellular senescence and cell cycle arrest through p53/p21 axis or p16INK4 activation[29,34]. SSL is also well known to have high rate of *BRAF* mutation[18]. Therefore, it is not uncommon to observe occasional eosinophilic atypical cells in SSLs[32]. Animal models supported that *BRAF* V600E mutation causes cellular senescence after first wave of proliferation[35] and a shift of balance from proliferation to differentiation, which can be rescued by a loss of additional differentiation-promoting factors (CDX2, SMAD4 and p16) or activation of WNT signaling[36]. In SSLs and TSAs located in proximal colon, hypermethylation of *P16INK4* promoter and loss of p16 expression are the late events[12] that may cause evasion of senescence program implemented by *BRAF* mutation, whereas activation of WNT is likely the pathway employed for the progression of distally located TSAs.

ECF is a key feature of TSAs, especially in large protuberant ones in the distal colon. The presence of ECF in TSAs ranges from 67% to 89%, depending on the location and size of the polyps[8,12,20]. ECF is defined as small crypts displaced from muscularis mucosa, likely representing a progression step by disrupting the signalings of colonic crypt homeostasis. Bone morphogenetic protein (BMP4) signaling is probably a good candidate. BMP signaling plays an important role in villus morphogenesis and is known to promote cell differentiation and repress crypt formation[37,38]. Studies using human pluripotent stem cells demonstrated that BMP signaling is only transiently required for colonic differentiation, while small intestinal differentiation is the default program in the absence of BMP signaling[10]. Loss of BMP signaling in animal model[37] leads to ectopic crypt foci that resembles the phenotype of juvenile polyposis syndrome, which is known to harbor *BMPR1A* and *SMAD4* mutations in human[39,40]. Therefore, it is possible that ECF and villiform growth of TSA represent dysplastic transformation of colonic crypts into small intestinal villous morphology. This morphology may arise owing to aberrant molecular pathways such as BMP signaling, which controls villus-crypt homeostasis of gastrointestinal tract. Along with early events of *BRAF* or *KRAS* mutation, additional molecular changes drive proliferation of intestinal epithelium and shape them into TSA with distinct cytomorphology. Further accumulations of aberration in p53 and WNT signaling lead to progression of TSA into prominent dysplasia and CRC.

CONCLUSION

TSAs are rare serrated polyps located predominantly in the distal colon. At least two pathways have been identified, converging on activation of MAPK by *BRAF* or *KRAS* mutations. Small HP/SSL-like lesions with *BRAF* mutations might initiate as TSA precursors. Whether it is the same case occurring in the small serrated lesion with *KRAS* mutation awaits further investigation. Because TSA-derived colorectal cancer is considered very aggressive[30], study of the TSA-carcinoma sequence, its progression from lack of dysplasia to high-grade atypia and malignancy, is also warranted in the future.

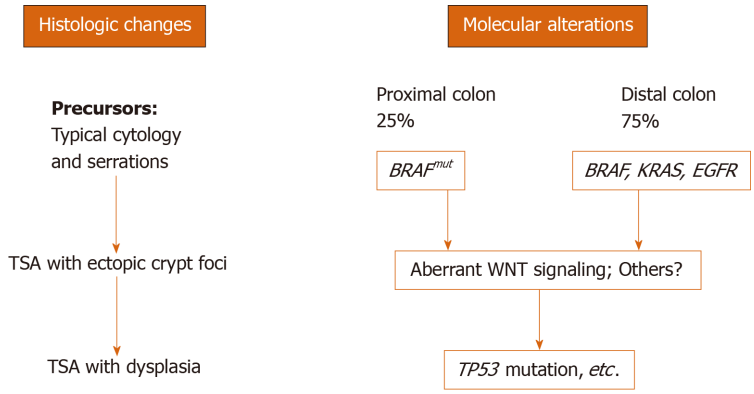

Figure 2 Histologic changes of traditional serrated adenoma parallel molecular alterations. During traditional serrated adenoma (TSA) development, mutations in *BRAF* (*BRAF*^{mut}), *KRAS* and *EGFR* cause typical cytomorphology and serration in precursor lesions. Accumulation of molecular alterations such as aberrant WNT signaling leads to fully developed TSA. Other pathways (Bone morphogenetic protein?) in addition to WNT signaling might also be involved in this step. Finally, mutations such as *TP53* will cause the progression of TSA into high-grade dysplasia and malignant transformation.

REFERENCES

1 **Bettington M**, Walker N, Clouston A, Brown I, Leggett B, Whitehall V. The serrated pathway to colorectal carcinoma: current concepts and challenges. *Histopathology* 2013; **62**: 367-386 [PMID: 23339363 DOI: 10.1111/his.12055]
2 **Snover DC**. Update on the serrated pathway to colorectal carcinoma. *Hum Pathol* 2011; **42**: 1-10 [PMID: 20869746 DOI: 10.1016/j.humpath.2010.06.002]
3 **Nagtegaal ID**, Odze RD, Klimstra D, Paradis V, Rugge M, Schirmacher P, Washington KM, Carneiro F, Cree IA; WHO Classification of Tumours Editorial Board. The 2019 WHO classification of tumours of the digestive system. *Histopathology* 2020; **76**: 182-188 [PMID: 31433515 DOI: 10.1111/his.13975]
4 **Bettington M**, Walker N, Rosty C, Brown I, Clouston A, Wockner L, Whitehall V, Leggett B. Critical appraisal of the diagnosis of the sessile serrated adenoma. *Am J Surg Pathol* 2014; **38**: 158-166 [PMID: 24418851 DOI: 10.1097/PAS.0000000000000103]
5 **Higuchi T**, Sugihara K, Jass JR. Demographic and pathological characteristics of serrated polyps of colorectum. *Histopathology* 2005; **47**: 32-40 [PMID: 15982321 DOI: 10.1111/j.1365-2559.2005.02180.x]
6 **Spring KJ**, Zhao ZZ, Karamatic R, Walsh MD, Whitehall VL, Pike T, Simms LA, Young J, James M, Montgomery GW, Appleyard M, Hewett D, Togashi K, Jass JR, Leggett BA. High prevalence of sessile serrated adenomas with BRAF mutations: a prospective study of patients undergoing colonoscopy. *Gastroenterology* 2006; **131**: 1400-1407 [PMID: 17101316 DOI: 10.1053/j.gastro.2006.08.038]
7 **Sweetser S**, Smyrk TC, Sinicrope FA. Serrated colon polyps as precursors to colorectal cancer. *Clin Gastroenterol Hepatol* 2013; **11**: 760-767; quiz e54-55 [PMID: 23267866 DOI: 10.1016/j.cgh.2012.12.004]
8 **Kim MJ**, Lee EJ, Suh JP, Chun SM, Jang SJ, Kim DS, Lee DH, Lee SH, Youk EG. Traditional serrated adenoma of the colorectum: clinicopathologic implications and endoscopic findings of the precursor lesions. *Am J Clin Pathol* 2013; **140**: 898-911 [PMID: 24225759 DOI: 10.1309/AJCPDJC9VC5KTYUS]
9 **Childs BG**, Baker DJ, Kirkland JL, Campisi J, van Deursen JM. Senescence and apoptosis: dueling or complementary cell fates? *EMBO Rep* 2014; **15**: 1139-1153 [PMID: 25312810 DOI: 10.15252/embr.201439245]
10 **Múnera JO**, Sundaram N, Rankin SA, Hill D, Watson C, Mahe M, Vallance JE, Shroyer NF, Sinagoga KL, Zarzoso-Lacoste A, Hudson JR, Howell JC, Chatuvedi P, Spence JR, Shannon JM, Zorn AM, Helmrath MA, Wells JM. Differentiation of Human Pluripotent Stem Cells into Colonic Organoids via Transient Activation of BMP Signaling. *Cell Stem Cell* 2017; **21**: 51-64.e6 [PMID: 28648364 DOI: 10.1016/j.stem.2017.05.020]
11 **Chetty R**. Traditional serrated adenoma (TSA): morphological questions, queries and quandaries. *J Clin Pathol* 2016; **69**: 6-11 [PMID: 26553935 DOI: 10.1136/jclinpath-2015-203452]
12 **Bettington ML**, Walker NI, Rosty C, Brown IS, Clouston AD, McKeone DM, Pearson SA, Klein K, Leggett BA, Whitehall VL. A clinicopathological and molecular analysis of 200 traditional serrated adenomas. *Mod Pathol* 2015; **28**: 414-427 [PMID: 25216220 DOI: 10.1038/modpathol.2014.122]
13 **Tsai JH**, Liau JY, Lin YL, Lin LI, Cheng YC, Cheng ML, Jeng YM. Traditional serrated adenoma has two pathways of neoplastic progression that are distinct from the sessile serrated pathway of colorectal carcinogenesis. *Mod Pathol* 2014; **27**: 1375-1385 [PMID: 24603588 DOI: 10.1038/modpathol.2014.35]
14 **Fu B**, Yachida S, Morgan R, Zhong Y, Montgomery EA, Iacobuzio-Donahue CA. Clinicopathologic and genetic characterization of traditional serrated adenomas of the colon. *Am J Clin Pathol* 2012; **138**: 356-366 [PMID: 22912351 DOI: 10.1309/AJCPVT7LC4CRPZSK]
15 **Sekine S**, Ogawa R, Hashimoto T, Motohiro K, Yoshida H, Taniguchi H, Saito Y, Yasuhiro O, Ochiai A, Hiraoka N. Comprehensive characterization of RSPO fusions in colorectal traditional serrated adenomas. *Histopathology* 2017; **71**: 601-609 [PMID: 28543708 DOI: 10.1111/his.13265]
16 **Bongers G**, Muniz LR, Pacer ME, Iuga AC, Thirunarayanan N, Slinger E, Smit MJ, Reddy EP, Mayer L, Furtado GC, Harpaz N, Lira SA. A role for the epidermal growth factor receptor signaling in development of intestinal serrated polyps in mice and humans. *Gastroenterology* 2012; **143**: 730-740 [PMID: 22643351 DOI: 10.1053/j.gastro.2012.05.034]
17 **Barras D**. BRAF Mutation in Colorectal Cancer: An Update. *Biomark Cancer* 2015; **7**: 9-12 [PMID: 26396549 DOI: 10.4137/BIC.S25248]
18 **Yang HM**, Mitchell JM, Sepulveda JL, Sepulveda AR. Molecular and histologic considerations in the

assessment of serrated polyps. *Arch Pathol Lab Med* 2015; **139**: 730-741 [PMID: 26030242 DOI: 10.5858/arpa.2014-0424-RA]

19 **Aoki H**, Yamamoto E, Takasawa A, Niinuma T, Yamano HO, Harada T, Matsushita HO, Yoshikawa K, Takagi R, Harada E, Tanaka Y, Yoshida Y, Aoyama T, Eizuka M, Yorozu A, Kitajima H, Kai M, Sawada N, Sugai T, Nakase H, Suzuki H. Epigenetic silencing of *SMOC1* in traditional serrated adenoma and colorectal cancer. *Oncotarget* 2018; **9**: 4707-4721 [PMID: 29435136 DOI: 10.18632/oncotarget.23523]

20 **Bettington M**, Rosty C, Whitehall V, Leggett B, McKeone D, Pearson SA, Walker N. A morphological and molecular study of proposed early forms of traditional serrated adenoma. *Histopathology* 2018; **73**: 1023-1029 [PMID: 30007084 DOI: 10.1111/his.13714]

21 **Wiland HO 4th**, Shadrach B, Allende D, Carver P, Goldblum JR, Liu X, Patil DT, Rybicki LA, Pai RK. Morphologic and molecular characterization of traditional serrated adenomas of the distal colon and rectum. *Am J Surg Pathol* 2014; **38**: 1290-1297 [PMID: 25127095 DOI: 10.1097/PAS.0000000000000253]

22 **Lu SH**, Yuan RH, Chen YL, Hsu HC, Jeng YM. Annexin A10 is an immunohistochemical marker for adenocarcinoma of the upper gastrointestinal tract and pancreatobiliary system. *Histopathology* 2013; **63**: 640-648 [PMID: 24024557 DOI: 10.1111/his.12229]

23 **Gonzalo DH**, Lai KK, Shadrach B, Goldblum JR, Bennett AE, Downs-Kelly E, Liu X, Henricks W, Patil DT, Carver P, Na J, Gopalan B, Rybicki L, Pai RK. Gene expression profiling of serrated polyps identifies annexin A10 as a marker of a sessile serrated adenoma/polyp. *J Pathol* 2013; **230**: 420-429 [PMID: 23595865 DOI: 10.1002/path.4200]

24 **Tsai JH**, Lin YL, Cheng YC, Chen CC, Lin LI, Tseng LH, Cheng ML, Liau JY, Jeng YM. Aberrant expression of annexin A10 is closely related to gastric phenotype in serrated pathway to colorectal carcinoma. *Mod Pathol* 2015; **28**: 268-278 [PMID: 25081749 DOI: 10.1038/modpathol.2014.96]

25 **Clevers H**. The intestinal crypt, a prototype stem cell compartment. *Cell* 2013; **154**: 274-284 [PMID: 23870119 DOI: 10.1016/j.cell.2013.07.004]

26 **Gehart H**, Clevers H. Tales from the crypt: new insights into intestinal stem cells. *Nat Rev Gastroenterol Hepatol* 2019; **16**: 19-34 [PMID: 30429586 DOI: 10.1038/s41575-018-0081-y]

27 **Sekine S**, Yamashita S, Tanabe T, Hashimoto T, Yoshida H, Taniguchi H, Kojima M, Shinmura K, Saito Y, Hiraoka N, Ushijima T, Ochiai A. Frequent PTPRK-RSPO3 fusions and RNF43 mutations in colorectal traditional serrated adenoma. *J Pathol* 2016; **239**: 133-138 [PMID: 26924569 DOI: 10.1002/path.4709]

28 **Hashimoto T**, Ogawa R, Yoshida H, Taniguchi H, Kojima M, Saito Y, Sekine S. Acquisition of WNT Pathway Gene Alterations Coincides With the Transition From Precursor Polyps to Traditional Serrated Adenomas. *Am J Surg Pathol* 2019; **43**: 132-139 [PMID: 30179900 DOI: 10.1097/PAS.0000000000001149]

29 **Bennecke M**, Kriegl L, Bajbouj M, Retzlaff K, Robine S, Jung A, Arkan MC, Kirchner T, Greten FR. Ink4a/Arf and oncogene-induced senescence prevent tumor progression during alternative colorectal tumorigenesis. *Cancer Cell* 2010; **18**: 135-146 [PMID: 20708155 DOI: 10.1016/j.ccr.2010.06.013]

30 **Bettington ML**, Chetty R. Traditional serrated adenoma: an update. *Hum Pathol* 2015; **46**: 933-938 [PMID: 26001333 DOI: 10.1016/j.humpath.2015.04.002]

31 **Feng Y**, Bommer GT, Zhao J, Green M, Sands E, Zhai Y, Brown K, Burberry A, Cho KR, Fearon ER. Mutant KRAS promotes hyperplasia and alters differentiation in the colon epithelium but does not expand the presumptive stem cell pool. *Gastroenterology* 2011; **141**: 1003-1013.e1-10 [PMID: 21699772 DOI: 10.1053/j.gastro.2011.05.007]

32 **Torlakovic EE**, Gomez JD, Driman DK, Parfitt JR, Wang C, Benerjee T, Snover DC. Sessile serrated adenoma (SSA) vs. traditional serrated adenoma (TSA). *Am J Surg Pathol* 2008; **32**: 21-29 [PMID: 18162766 DOI: 10.1097/PAS.0b013e318157f002]

33 **Cassese G**, Amendola A, Maione F, Giglio MC, Pagano G, Milone M, Aprea G, Luglio G, De Palma GD. Serrated Lesions of the Colon-Rectum: A Focus on New Diagnostic Tools and Current Management. *Gastroenterol Res Pract* 2019; **2019**: 9179718 [PMID: 30774654 DOI: 10.1155/2019/9179718]

34 **Endo A**, Koizumi H, Takahashi M, Tamura T, Tatsunami S, Watanabe Y, Takagi M. A significant imbalance in mitosis versus apoptosis accelerates the growth rate of sessile serrated adenoma/polyps. *Virchows Arch* 2013; **462**: 131-139 [PMID: 23292000 DOI: 10.1007/s00428-012-1365-1]

35 **Carragher LA**, Snell KR, Giblett SM, Aldridge VS, Patel B, Cook SJ, Winton DJ, Marais R, Pritchard CA. V600EBraf induces gastrointestinal crypt senescence and promotes tumour progression through enhanced CpG methylation of p16INK4a. *EMBO Mol Med* 2010; **2**: 458-471 [PMID: 20941790 DOI: 10.1002/emmm.201000099]

36 **Tong K**, Pellón-Cárdenas O, Sirihorachai VR, Warder BN, Kothari OA, Perekatt AO, Fokas EE, Fullem RL, Zhou A, Thackray JK, Tran H, Zhang L, Xing J, Verzi MP. Degree of Tissue Differentiation Dictates Susceptibility to BRAF-Driven Colorectal Cancer. *Cell Rep* 2017; **21**: 3833-3845 [PMID: 29281831 DOI: 10.1016/j.celrep.2017.11.104]

37 **Haramis AP**, Begthel H, van den Born M, van Es J, Jonkheer S, Offerhaus GJ, Clevers H. De novo crypt formation and juvenile polyposis on BMP inhibition in mouse intestine. *Science* 2004; **303**: 1684-1686 [PMID: 15017003 DOI: 10.1126/science.1093587]

38 **He XC**, Zhang J, Tong WG, Tawfik O, Ross J, Scoville DH, Tian Q, Zeng X, He X, Wiedemann LM, Mishina Y, Li L. BMP signaling inhibits intestinal stem cell self-renewal through suppression of Wnt-beta-catenin signaling. *Nat Genet* 2004; **36**: 1117-1121 [PMID: 15378062 DOI: 10.1038/ng1430]

39 **Howe JR**, Sayed MG, Ahmed AF, Ringold J, Larsen-Haidle J, Merg A, Mitros FA, Vaccaro CA, Petersen GM, Giardiello FM, Tinley ST, Aaltonen LA, Lynch HT. The prevalence of MADH4 and BMPR1A mutations in juvenile polyposis and absence of BMPR2, BMPR1B, and ACVR1 mutations. *J Med Genet* 2004; **41**: 484-491 [PMID: 15235019 DOI: 10.1136/jmg.2004.018598]

40 **Woodford-Richens K**, Bevan S, Churchman M, Dowling B, Jones D, Norbury CG, Hodgson SV, Desai D, Neale K, Phillips RK, Young J, Leggett B, Dunlop M, Rozen P, Eng C, Markie D, Rodriguez-Bigas MA, Sheridan E, Iwama T, Eccles D, Smith GT, Kim JC, Kim KM, Sampson JR, Evans G, Tejpar S, Bodmer WF, Tomlinson IP, Houlston RS. Analysis of genetic and phenotypic heterogeneity in juvenile polyposis. *Gut* 2000; **46**: 656-660 [PMID: 10764709 DOI: 10.1136/gut.46.5.656]

World Journal of Gastrointestinal Pathophysiology

Submit a Manuscript: https://www.f6publishing.com

World J Gastrointest Pathophysiol 2020 June 20; 11(4): 84-103

DOI: 10.4291/wjgp.v11.i4.84

ISSN 2150-5330 (online)

ORIGINAL ARTICLE

Basic Study

P2X7 receptor antagonist recovers ileum myenteric neurons after experimental ulcerative colitis

Roberta Figueiroa Souza, Mariá Munhoz Evangelinellis, Cristina Eusébio Mendes, Marta Righetti, Múcio Cevulla Silva Lourenço, Patricia Castelucci

ORCID number: Roberta Figueiroa Souza (0000-0003-4380-6373); Mariá Munhoz Evangelinellis (0000-0002-2594-437X); Cristina Eusébio Mendes (0000-0003-3534-6282); Marta Righetti (0000-0002-0963-9893); Múcio Cevulla Silva Lourenço (0000-0002-3466-7976); Patricia Castelucci (0000-0002-7475-5962).

Author contributions: Souza RF performed the immunohistochemistry experiments and analyzed the results; Evangelinellis MM and Mendes CE helped with inflammation and BBG protocols; Righetti M and Lourenço MCS performed the histological protocols; Castelucci P planned experiments, analyzed the results, and wrote and edited the manuscript.

Supported by Foundation São Paulo Research, No. 2014/25927-2 and No. 2018/07862-1; Coordenação de Aperfeiçoamento de Pessoal de Nível Superior; and Conselho Nacional de Desenvolvimento Científico e Tecnológico.

Institutional animal care and use committee statement: This study was approved by the Institute of Biomedical and Sciences/an Faculty of Veterinary Medicine and Animal Science, University of São Paulo, Protocol number # 1793240815. The animal experiments in this study were conducted according to the current regulations of the Ethics

Roberta Figueiroa Souza, Cristina Eusébio Mendes, Marta Righetti, Múcio Cevulla Silva Lourenço, Patricia Castelucci, Department of Anatomy, University of São Paulo, São Paulo 05508-900, Brazil

Mariá Munhoz Evangelinellis, Department of Surgery, Faculty of Veterinary Medicine and Animal Science, University of São Paulo, São Paulo 05508-900, Brazil

Corresponding author: Patricia Castelucci, PhD, Associate Professor, Department of Anatomy, University of São Paulo, Lineu Prestes, 2415, São Paulo 05508-900, Brazil. pcastel@usp.br

Abstract

BACKGROUND

The P2X7 receptor is expressed by enteric neurons and enteric glial cells. Studies have demonstrated that administration of a P2X7 receptor antagonist, brilliant blue G (BBG), prevents neuronal loss.

AIM

To report the effects of BBG in ileum enteric neurons immunoreactive (ir) following experimental ulcerative colitis in *Rattus norvegicus albinus*.

METHODS

2,4,6-trinitrobenzene sulfonic acid (TNBS group, $n = 5$) was injected into the distal colon. BBG (50 mg/kg, BBG group, $n = 5$) or vehicle (sham group, $n = 5$) was given subcutaneously 1 h after TNBS. The animals were euthanized after 24 h, and the ileum was removed. Immunohistochemistry was performed on the myenteric plexus to evaluate immunoreactivity for P2X7 receptor, neuronal nitric oxide synthase (nNOS), choline acetyltransferase (ChAT), HuC/D and glial fibrillary acidic protein.

RESULTS

The numbers of nNOS-, ChAT-, HuC/D-ir neurons and glial fibrillary acidic protein-ir glial cells were decreased in the TNBS group and recovered in the BBG group. The neuronal profile area (μm^2) demonstrated that nNOS-ir neurons decreased in the TNBS group and recovered in the BBG group. There were no differences in the profile areas of ChAT- and HuC/D-ir neurons.

CONCLUSION

Our data conclude that ileum myenteric neurons and glial cells were affected by

Committee on Animal Use of the Biomedical Science Institute of the University of São Paulo. Furthermore, all protocols were approved by the Ethics Committee on Animal Use of the Biomedical Science Institute of the University of São Paulo (Protocol 68/2016).

Conflict-of-interest statement: The authors have no conflicts of interest.

Data sharing statement: No additional data are available.

ARRIVE guidelines statement: The authors have read the ARRIVE guidelines, and the manuscript was prepared and revised according to the ARRIVE guidelines.

Manuscript source: Invited manuscript

Received: January 7, 2020
Peer-review started: January 7, 2020
First decision: February 19, 2020
Revised: April 4, 2020
Accepted: April 18, 2020
Article in press: April 18, 2020
Published online: June 20, 2020

P-Reviewer: Mihara H, Yamamoto S
S-Editor: Wang YQ
L-Editor: A
E-Editor: Qi LL

ulcerative colitis and that treatment with BBG had a neuroprotective effect. Thus, these results demonstrate that the P2X7 receptor may be an important target in therapeutic strategies.

Key words: P2X7 receptor; Brilliant blue G; Myenteric plexus; Experimental ulcerative colitis; Ileum; Chemical coding

Core tip: This work aims to analyze the effects of experimental ulcerative colitis (EUC) in ileum myenteric neurons immunoreactive (ir) for P2X7 receptor, neuronal nitric oxide synthase, choline acetyltransferase, HuC/D and enteric glial cells immunoreactive for glial fibrillary acidic protein. The animals were treated with P2X7 receptor antagonist, brilliant blue G (BBG). The results showed that the numbers of neuronal nitric oxide synthase-, choline acetyltransferase-, HuC/D-ir neurons and glial fibrillary acidic protein-ir glial cells were decreased in the EUC group and recovered in the animals treated with BBG. BBG treatment demonstrated that the P2X7 receptor may be a possible therapeutic target in the treatment of the EUC.

Citation: Souza RF, Evangelinellis MM, Mendes CE, Righetti M, Lourenço MCS, Castelucci P. P2X7 receptor antagonist recovers ileum myenteric neurons after experimental ulcerative colitis. *World J Gastrointest Pathophysiol* 2020; 11(4): 84-103
URL: https://www.wjgnet.com/2150-5330/full/v11/i4/84.htm
DOI: https://dx.doi.org/10.4291/wjgp.v11.i4.84

INTRODUCTION

The enteric nervous system (SNE) performs functions in gastrointestinal tract motility, control of gastric acid secretion, regulation of fluid movement through the epithelium, changes in local blood flow, and interactions with the endocrine and intestinal immune systems[1,2]. This system has two ganglionic plexuses, the myenteric plexus and the submucosal plexus. The myenteric plexus is located between the outer longitudinal muscular layer and the circular muscle layer, extending throughout the digestive tract from the esophagus to the rectum. The submucosal plexus is found predominantly in the small and large intestines and has a smaller ganglion, and its interconnected fibers are thinner compared to those of the myenteric plexus[1,2]. Enteric glial cells have functions to support neurons, regulate synaptic transmission, and release cytokines[3,4].

Inflammatory bowel diseases (IBDs) are disorders that affect the digestive tract. These problems include ulcerative colitis and Crohn's disease[5]. There are changes in SNE populations in ulcerative colitis of animals and humans[6-10]. Additionally, McCready *et al*[11] described the expansion of the inflammatory process from the distal ileum.

Studies have shown that the release of ATP by enteric neurons as noncholinergic and nonadrenergic neurotransmitters may be related to intestinal motility[12-15]. Purinergic receptors are classified into P1 and P2, where P1 receptors are activated by the adenine nucleoside and P2 receptors are activated by the nucleotide ADP (adenosine diphosphate) or ATP[16]. P2X receptors are ion channels with selective permeability to Ca^{2+}, K^+ and Na^+ cations, and they can be found in the central nervous system, ENS and enteric glial cells[15,17,18]. Seven types of P2X receptors have been described: P2X1, P2X2, P2X3, P2X4, P2X5, P2X6 and P2X7[18-21].

The P2X7 receptor has been described in the ENS[22,23]. Studies show that brilliant blue G (BBG) is a P2X7 antagonist, and its low toxicity[24,25] and high selectivity make this compound an ideal candidate to block the adverse effects of P2X7 receptor activation[26]. P2X7 receptor-deficient animals have been shown to exhibit improvements in their overall condition when subjected to experimental ulcerative colitis[27]. Peng *et al*[28] demonstrated recovery of the rat spinal cord after mechanical injury following BBG administration. Additionally, Palombit *et al*[29] observed recovery of BBG-treated enteric neurons following an ischemia and reperfusion protocol.

This work aims to analyze the effects of experimental ulcerative colitis in neurons immunoreactive (ir) for neuronal nitric oxide synthase (nNOS), choline

acetyltransferase (ChAT) which is marker for intrinsic primary afferent neurons (IPANs) and excitatory motor neuron, and HuC/D (a pan-neuronal marker) and enteric glial cells immunoreactive for glial fibrillary acidic protein (GFAP) in the ileum in animals treated with BBG.

MATERIALS AND METHODS

The animal experiments in this study were conducted according to the current regulations of the Ethics Committee on Animal Use of the Biomedical Science Institute of the University of São Paulo. Furthermore, all protocols were approved by the Ethics Committee on Animal Use of the Biomedical Science Institute of the University of São Paulo (Protocol 68/2016). Young male Wistar rats (200–300 g body weight) were maintained under standard conditions at 21 °C with a 12-h light-dark cycle. All groups were supplied with water *ad libitum*.

Ulcerative colitis induction

The rats were anesthetized with a mixture of xylazine (20 mg/kg) and ketamine (100 mg/kg) administered subcutaneously. Inflammation was induced through the intrarectal insertion of a polypropylene 8 cm cannula. 2,4,6-trinitrobenzene sulfonic acid (TNBS, Sigma, Saint Louis, United States) was injected at a dose of 30 mg/kg in 600 μL of 30% ethanol in the colon lumen (n = 5). Sham animals (n = 5) were injected with vehicle. BBG (50 mg/kg, Sigma Aldrich, United Kingdom, n = 5) or saline was injected 1 h following TNBS injection (n = 5)[28,29]. The survival time after colitis induction was 24 h.

For macroscopic and microscopic analyses, colitis was assessed according to macroscopic colonic injury[30]. The scores were stratified as follows: 0 = normal, 1 = presence of hyperemia without ulcers, 2 = ulcerations without hyperemia, 3 = ulcerations at one site, 4 = two or more sites of ulcerations, 5 = sites of damage extending > 1 cm, and 6 to 10 = sites of damage extending > 2 cm, with the score increasing by 1 for each additional cm[30]. The microscopic colitis scores were assessed using a scoring system adapted from Erdogan *et al*[31] and Fabia *et al*[32]. The scores were categorized as follows according to the corresponding parameters. Ulcerations: 0 = no ulcer, 1 = single ulceration not exceeding the lamina muscularis mucosa, 2 = ulcerations not exceeding the mucosa, and 3 = ulcerations exceeding the submucosa. Edema (submucosa): 0 = no edema, 1 = mild edema, 2 = moderate edema, and 3 = severe edema. Inflammatory cell infiltration: 0 = no infiltration, 1 = mild infiltration, 2 = moderate infiltration, and 3 = dense infiltration.

The scoring of the disease activity index (DAI) was analyzed in the control, sham and colitis rats. Percentage weight change, stool consistency and/or presence of occult bleeding were examined. The scores were categorized as follows according to the corresponding parameters. Weight change (%) score: 0 = 1%, 1 = 1%-5%, 2 = 5%-10%, 3 = 10%-15%, and 4 = > 15%. Stool consistency (%) score: 0 = normal[a] (well-formed pellets), 1 = normal, 2 = loose stool[b] (pasty and semiformed stools that do not stick to the anus), 3 = loose stool, and 4 = diarrhea[c] (liquid stools that stick to the anus). Occult/gross rectal bleeding: 0 = normal, 1 = occult blood +, 2 = occult blood ++, 3 = occult blood +++, and 4 = gross bleeding. The disease activity index was calculated by summing the score parameters[7,33,34].

Immunohistochemistry

For immunohistochemistry, fresh segments of the ileum were dissected and placed in PBS containing nicardipine (10^{-6} mol/L, Sigma, United States) to inhibit tissue contraction. The segments were opened along the mesenteric border and cleaned with PBS. The tissues were then placed mucosal side down onto a sheet of balsa wood and fixed overnight at 4 °C with 4% paraformaldehyde in sodium phosphate buffer 0.2 mol/L (pH 7.3). The next day, the tissue was cleared of fixative with three 10-min washes in 100% dimethyl sulfoxide (DMSO), followed by three 10-min washes in PBS. All tissue was stored at 4 °C in PBS containing sodium azide (0.1%). The tissue collection was performed by the same researcher who placed the tissue onto the balsa board to be fixed (see material and methods). The processing maintained the same stretch between preparations.

The fixed tissue was subdissected to remove the mucosal and circular layers, producing only the longitudinal muscle layer with the myenteric plexus. For immunohistochemistry, the myenteric plexus of the ileum was preincubated with 10% normal horse serum in PBS containing 1.5% Triton X-100 for 45 min at room temperature. The antibodies used in this study are listed in Table 1. Double labeling was achieved using combinations of the antisera indicated in Table 1. After incubation with primary antisera, tissues were washed three times for 10 min each time in PBS

and incubated with various secondary antibodies (Table 1). The PBS washes were repeated, and the tissue was mounted in buffered glycerol with 0.5 mol/L sodium carbonate (pH 8.6).

The stained tissue specimens were examined using a Nikon 80i fluorescent microscope. The images were captured using a digital camera and the NIS Nikon software package. Additionally, the tissue specimens were analyzed using confocal microscopy on a Zeiss confocal scanning laser system installed on a Zeiss Axioplan 2 microscope. Images were taken at 512 × 512 pixels, and the thickness of each optical section was 0.5 μm. Z-stacks of ir cells were captured as a series of optical sections with a center spacing of 0.2 μm. The confocal images were collected using LSM 5 Image Zeiss processing software and were further processed using Corel Photo Paint and Corel Draw software.

Histological analysis

Samples of ileum and distal colon from the sham (n = 3), TNBS (n = 3) and BBG (n = 3) groups were washed in PBS, opened at the mesenteric border, placed on balsa wood and fixed in 4% paraformaldehyde for 48 h. The tissues were treated in increasing concentrations of alcohol, cleared in xylene and embedded in Paraplast Plus® (Sigma). The tissues were cut (5 mm) and stained with hematoxylin-eosin (HE). Qualitative analysis was performed to observe changes caused by experimental ulcerative colitis. For analyzes it was used a Nikon 80i microscope coupled to a camera with NIS-Elements AR 3.1 (Nikon) software.

Quantitative analysis

The analyzes were also done by double marking the membrane preparations on the Nikon 80i fluorescence microscope. First, the neurons were located by the presence of the fluorophore that marks an antigen and then the filter was changed to determine whether or not the neuron was marked by a second antigen, located by a second fluorophore of a different color. The cohort size was 100 neurons, and the data were collected from preparations obtained from five animals. The percentages of double-ir neurons were calculated and expressed as the mean ± SE (n = number of preparations). In total, 100 neurons and 100 enteric glial cells from each membrane preparation were analyzed from each of the sham (n = 5), TNBS (n = 5) and BBG (n = 5) groups[7,29]. The density of neurons (neurons/cm^2) ir for P2X7, nNOS, ChAT, anti-HuC/D (pan-neuronal marker) and GFAP (pan-glial cells) as well as the neuronal morphological profiles was measured by analyzing all of the samples at 100 × magnification. Counts were made in 40 microscopic fields (0.000379 cm^2) for each antigen in a zig-zag pattern to avoid counting the same area more than once for each antigen in each animal, and a total of 200 microscopic fields were analyzed per immunoreactivity. Cell profile areas (μm^2) were obtained for 100 randomly selected neurons in two whole-mount preparations per animal per nNOS, ChAT, anti-HuC/D immunoreactivity assay from 5 rats for each group. A total of 500 neurons per group were analyzed using a Nikon 80i microscope coupled to a camera with NIS-Elements AR 3.1 (Nikon) software and were measured using Image-Pro Plus software version 4.1.0.0. Data were compared by analysis of variance (ANOVA) and Tukey's test for multiple comparisons, as appropriate. $P < 0.05$ was considered statistically significant.

RESULTS

On histological analysis, the ileum showed no lesions and had a normal appearance in the sham, TNBS and BBG groups (Table 2). However, the histological observations showed that in distal colon the edema and inflammatory cell infiltration in the TNBS group. The mucosa, the circular and longitudinal muscles and the distal colon enteric neurons in the Sham and BBG groups were preserved. Additionally, the microscopic scores did not indicate ulcerations, edema or inflammatory cell infiltration in the ileums of all groups (Table 2).

The DAI showed changes in weight (%), stool consistency (%) and occult/gross rectal bleeding (%) in the sham, TNBS and BBG groups (Figure 1). The results show that there was an increase in DAI scores, stool consistency and occult bleeding in the TNBS group and a recovery in the BBG group. Histological studies revealed that the mucosa, lamina propria and submucosal ganglia in all groups were not affected (Figure 2).

Immunohistochemical analysis showed that the P2X7 receptor was present in the myenteric neurons in the sham, TNBS and BBG groups. P2X7 receptor-ir neurons were labeled for HuC/D, nNOS, ChAT and GFAP in all groups studied (Figures 3, 4, 5 and 6). The P2X7 receptor immunoreactivity colocalized 100% with neurons positive for HuC/D, nNOS, ChAT and GFAP in all groups.

Table 1 Characteristics of primary and secondary antibodies

Antigen	Host	Dilution	Source
P2X7 receptor	Rabbit	1:200	Millipore (AB5246)
nNOS	Sheep	1:2000	Millipore (AB1529)
ChAT	Goat	1:50	Chemicon (AB144P)
Anti-HuC/D	Mouse	1:100	Molecular probes (A-21271)
GFAP	Rabbit	1:400	DAKO (Z0334)
GFAP	Mouse	1:200	Sigma (G3893)
Secondary antibodies			
Donkey anti-rabbit IgG 488		1:500	Molecular probes (A21206)
Donkey anti-sheep IgG 594		1:100	Molecular probes (A11016)
Donkey anti-mouse IgG 594		1:200	Molecular probes (A21203)

nNOS: Neuronal nitric oxide synthase; ChAT: Choline acetyltransferase; GFAP: Glial fibrillary acidic protein.

GFAP-positive glial cells were observed close to ChAT- and nNOS-immunoreactive neurons (Figures 7 and 8).

P2X7 receptor immunoreactivity per area of neurons decreased in the TNBS group by 10.6% compared to that in the sham group ($P < 0.05$). There was an increase of 20.4% in the BBG group compared to the TNBS group ($P < 0.01$) (Figure 9A).

nNOS-positive neurons per area decreased by 22.9% in the TNBS group compared to the sham group ($P < 0.05$). An increase of 22.2% was observed in the BBG group compared to the TNBS group ($P < 0.01$) (Figure 9B).

The ChAT-immunoreactive neurons per cm^2 were reduced by 34.0% in the TNBS group compared to the sham group ($P < 0.05$), and they were increased by 13.9% in the BBG group compared to the TNBS group ($P < 0.01$) (Figure 9C).

HuC/D-immunoreactive neurons per area reduced by 15.4% in the TNBS group compared to the sham group ($P < 0.05$). Furthermore, there was an increase of 19.5% in the BBG group compared to the TNBS group ($P < 0.01$) (Figure 9D).

The GFAP-positive enteric glial cells per cm^2 reduced by 14.4% in the TNBS group compared to the sham group ($P < 0.05$), and there was an increase of 17.7% in enteric glia in the BBG group compared to the TNBS group ($P < 0.01$) (Figure 9E).

Regarding neuronal profile area, the nNOS profile area decreased by 12% in the TNBS group compared to the sham group ($P < 0.05$), and an increase of 8% was observed in the BBG group compared to the TNBS group ($P < 0.05$) (Figure 10A). No differences were observed between the ChAT- and HuC/D neuronal profile areas of the studied groups. Due to colocalization, the profile areas of P2X7-positive nerve cells in the myenteric plexus were not quantified (Figure 10).

The distribution of nNOS-positive neurons showed that the size ranged from 50 μm^2 to 1050 μm^2 and that 22% to 25% of neurons were between 150 μm^2 and 350 μm^2 in the sham, TNBS and TNBS groups (Figure 11A).

The immunoreactive ChAT neurons demonstrated that the range size ranged from 50 μm^2 to 950 μm^2, with 27% to 37% being between 150 μm^2 and 250 μm^2 in all groups (Figure 11B).

The distribution of HuC/D-positive neurons showed that the size ranged from 50 μm^2 to 850 μm^2, with 21% to 43% between 150 μm^2 and 250 μm^2 in all groups (Figure 11C).

DISCUSSION

The experimental ulcerative colitis model affected ileum myenteric plexus neurons, and these neurons recovered with the use of BBG. The colitis model established by injecting TNBS in ethanol solution is considered effective and is widely used in the literature to produce experimental ulcerative colitis[10,35]. From the DAI, it was possible to observe that the experimental ulcerative colitis affected the weight, change in stool consistency and occult/gross rectal bleeding, and the reduction in these parameters showed an improvement in the condition of the group treated with BBG.

In our work, macroscopic and microscopic analysis of the ileum did not show that the mucosa or submucosa were affected. However, the literature has shown that experimental ulcerative colitis presents superficial inflammation, limited to mucosal and submucosal regions in the distal colon[6,7,36].

Table 2 Macroscopic and microscopic scores of ileums from the sham, 2,4,6-trinitrobenzene sulfonic acid and brilliant blue G groups

Variables	Sham	TNBS	BBG
Macroscopic score	0	0	0
Microscopic score			
Ulcerations	0	0	0
Edema (submucosa)	0	0	0
Inflammatory cell infiltration	0	0	0

For macroscopic and microscopic analyses colitis was assessed according to colonic injury[30]. The scores were stratified as follows: 0 = normal, 1 = presence of hyperemia without ulcers, 2 = ulcerations without hyperemia, 3 = ulcerations at one site, 4 = two or more sites of ulcerations, 5 = sites of damage extending > 1 cm, and 6 to 10 = sites of damage extending > 2 cm, with the score increasing by 1 for each additional cm[30]. The microscopic colitis scores were assessed using a scoring system adapted from Erdogan *et al*[31] and Fabia *et al*[32]. The scores were categorized as follows according to the corresponding parameters. Ulcerations: 0 = no ulcer, 1 = single ulceration not exceeding the lamina muscularis mucosa, 2 = ulcerations not exceeding the mucosa, and 3 = ulcerations exceeding the submucosa. Edema (submucosa): 0 = no edema, 1 = mild edema, 2 = moderate edema, and 3 = severe edema. Inflammatory cell infiltration: 0 = no infiltration, 1 = mild infiltration, 2 = moderate infiltration, and 3 = dense infiltration[31,32]. TNBS: 2,4,6-trinitrobenzene sulfonic acid; BBG: Brilliant blue G.

Enteric neurons of the distal colon are affected by experimental ulcerative colitis and Crohn's disease[37-39]. In our study, we observed a decrease in nNOS, ChAT and HuC/D-positive neurons in the ileum, thus demonstrating that experimental colitis in the distal colon may affect neurons in locations distant from the origin of the lesion.

Immunohistochemical studies have demonstrated the expression of P2X7 receptors in the SNE[6,7,22]. Gulbransen *et al*[40] observed activation of P2X7 receptors during colitis. In our study, we observed P2X7 receptor immunoreactivity in ileum myenteric plexus cells in all groups. We also observed a reduction in the number of P2X7 receptor immunoreactive cells in the TNBS group compared to that in the sham group and recovery of the neurons in the BBG group. da Silva *et al*[6,7] observed a decrease in P2X7 receptor-positive cells in the distal colon following experimental ulcerative colitis.

Purinergic mechanisms may be involved in the etiology of many conditions that affect the nervous system, due the large extracellular release of ATP[41]. Changes in purinergic receptor expression in neurons are observed in neuronal maturation, differentiation, acute CNS injuries, such as hypoxia ischemia, mechanical stress and inflammation.

It was observed that experimental ulcerative colitis affected neuronal classes in the ileum. In this study, a decrease in nNOS-, ChAT- and HuC/D-immunoreactive neurons per μm^2 was observed, and the recovery of these neurons per μm^2 was observed with BBG treatment. It has been observed that several classes of enteric neurons are affected in Crohn's disease and experimental ulcerative colitis[8,38,39,42]. Studies have demonstrated that ischemia and reperfusion decrease the number of enteric neurons[23] and treatment with BBG, a P2X7 antagonist, recovers rat enteric neurons[29]. Additionally, transient receptor potential channel vanilloid 2 (TRPV2) and the release of nitric oxide (NO) are related to intestinal motility[43].

Enteric glial cells have different functions in the face of gastrointestinal disorders[44,45]. In our study, we observed a decrease in GFAP immunoreactive glia in the ileum of the TNBS group compared to that in the sham group and recovery in the BBG group.

The evaluation of morphometric changes (measurement of cell profile area) has been widely studied in several experimental protocols. In the present work, the analysis of the profile of the nNOS-, ChAT- and HuC/D-ir neurons was performed to determine changes in the profile areas in these neuronal classes. However, only nitrergic neurons of the TNBS group showed a decrease, and those treated with BBG demonstrated recovery. The increased neuronal profile area could be explained as a compensatory mechanism due to neuronal death in the TNBS group[6,29].

The literature elucidates the neuroprotective role of P2X7 receptor blockade, as well as a possible increase in the expression of anti-inflammatory factors IL-10 and TGF-β1 by KO P2X7 mice, expressly helping to control inflammation[27,29,46].

Studies have described that gastrointestinal epithelia release ATP and Transient Receptor Potential Vanilloid 4 (TRPV4) is expressed throughout the gastrointestinal epithelia[47].

The importance of this work is to demonstrate that experimental ulcerative colitis

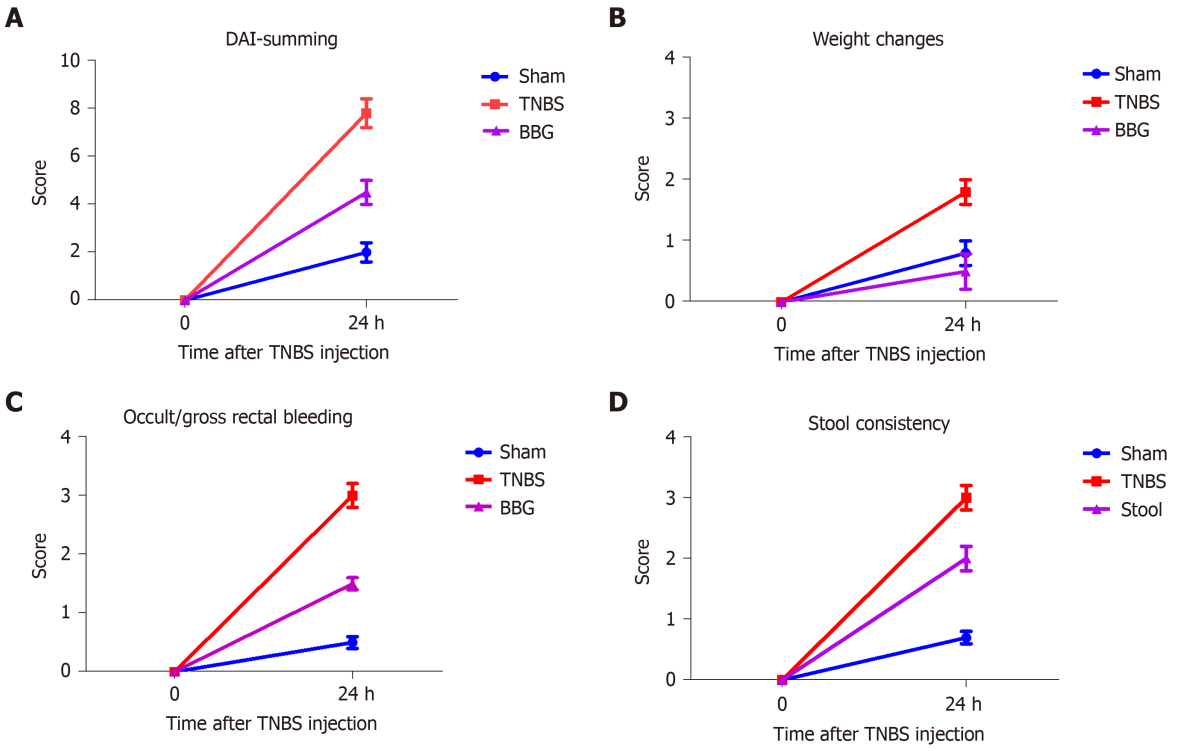

Figure 1 Scoring of the disease activity index in the in the sham, 2,4,6-trinitrobenzene sulfonic acid and brilliant blue G groups. A: The disease activity index was calculated by summing the score parameters: Mild activity was classified from 1 to 4; moderate activity, from 5 to 8; and maximal activity from 9 to 12. The scores were categorized as follows according to the corresponding parameters; B: Weight change score: 0 ≤ 1, 1 = 1-5, 2 = 5-10, 3 = 10-15, and 4 ≥ 15%; C: Occult/gross rectal bleeding: 0 = normal, 1 = occult blood +, 2 = occult blood ++, 3 = occult blood +++, and 4 = gross bleeding; D: Stool consistency score: 0 = normal (well-formed pellets), 1 = normal, 2 = loose stool (pasty and semiformed stools that do not stick to the anus), 3 = loose stool, and 4 = diarrhea (liquid stools that stick to the anus). DAI: Disease activity index; TNBS: 2,4,6-trinitrobenzene sulfonic acid; BBG: Brilliant blue G.

affects distant organs such as ileum myenteric neurons that express the P2X7 receptor. In addition, BBG treatment was shown to be effective in the recovery of ileum myenteric neurons, thus demonstrating that the P2X7 receptor may be a possible therapeutic target in the treatment of the effects of experimental ulcerative colitis. Also, has been described that the expansion of the inflammatory process from the distal neck to the distal ileum.

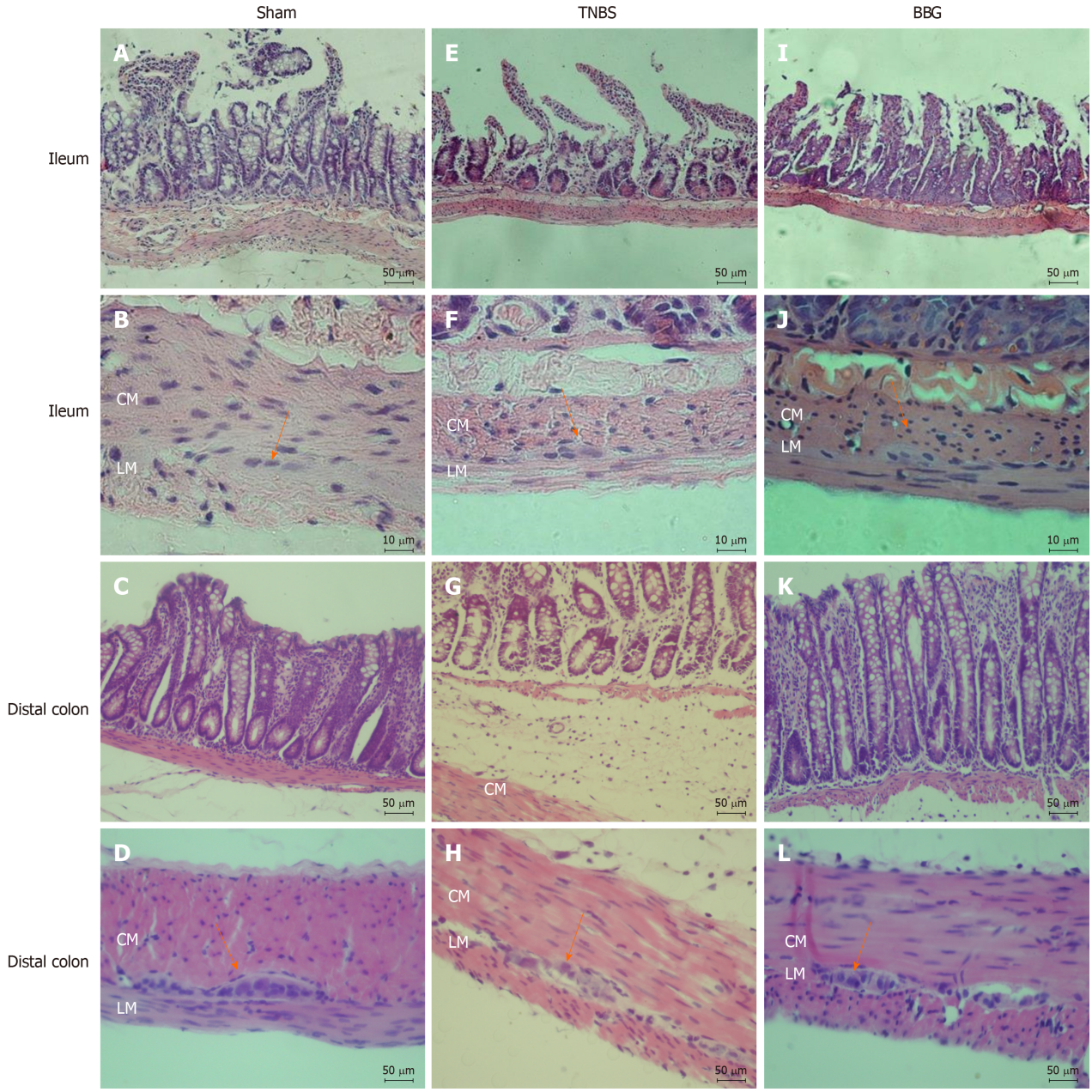

Figure 2 Photomicrographs showing sections stained with hematoxylin and eosin. A, B, E, F, I, J: Rat ileum myenteric plexus in the sham, 2,4,6-trinitrobenzene sulfonic acid (TNBS) and brilliant blue G (BBG) groups; C, D, G, H, K, L: Rat distal colon myenteric plexus in the sham, TNBS and BBG groups. The histological observations showed that in ileum the appearances of the mucosa, circular and longitudinal muscles and enteric neurons in the sham, TNBS and BBG groups were preserved. However, the histological observations showed that in distal colon the edema and inflammatory cell infiltration in the TNBS group. The mucosa, the circular and longitudinal muscles and the distal colon enteric neurons in the sham and BBG groups were preserved. Orange arrows indicate myenteric ganglia. CM: Circular muscle; LM: Longitudinal plexus; TNBS: 2,4,6-trinitrobenzene sulfonic acid; BBG: Brilliant blue G. Scale bars: A, C, D, E, G, H, I, K, L = 50 μm; B, F, J = 10 μm.

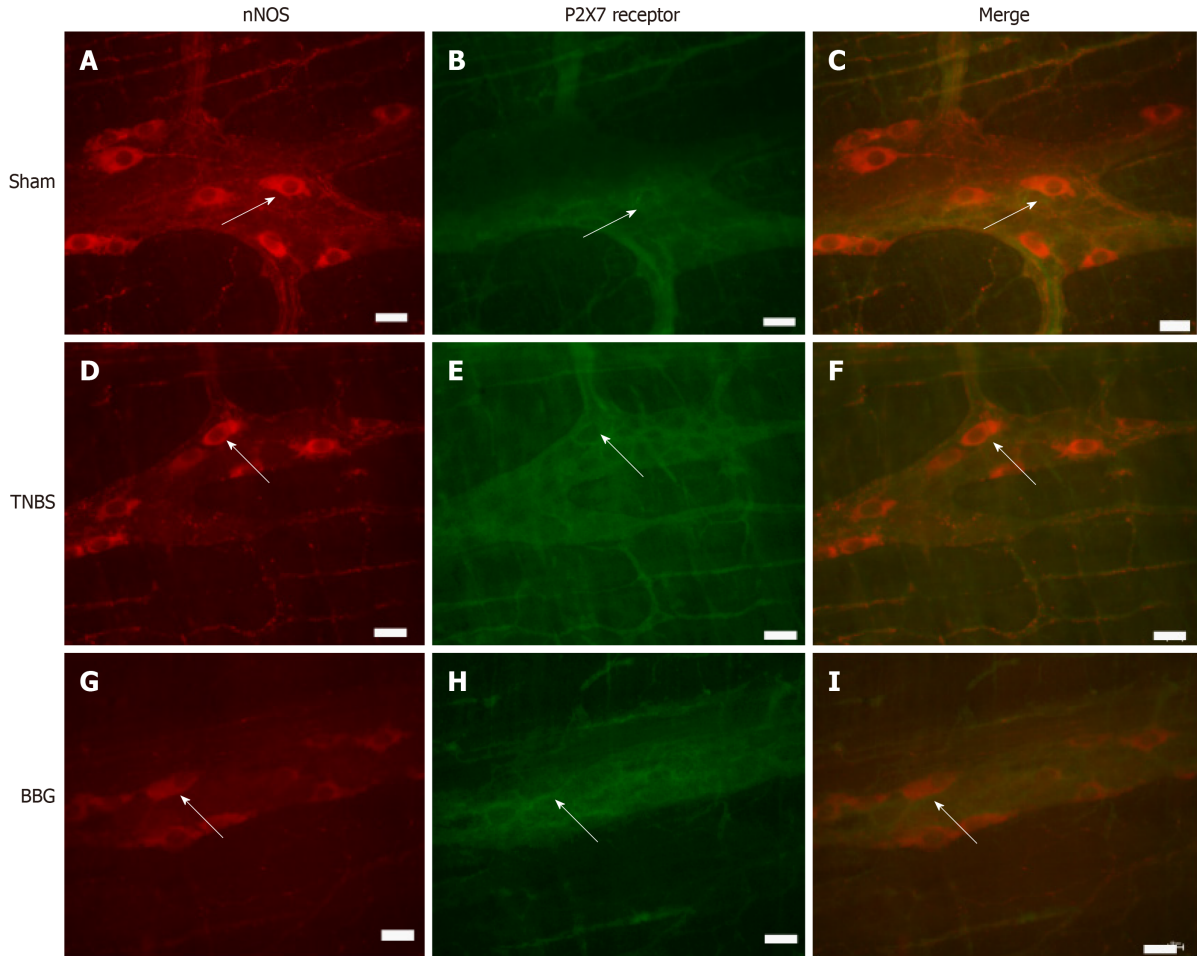

Figure 3 Colocalization of the P2X7 receptor with neuronal nitric oxide synthase in neurons of the rat ileum myenteric plexus in the sham, 2,4,6-trinitrobenzene sulfonic acid and brilliant blue G groups. A-C: Sham group; D-F: 2,4,6-trinitrobenzene group; G-I: Brilliant blue G group. Neuronal nitric oxide synthase immunoreactivity (red; A, D, and G) colocalized with P2X7 immunoreactivity (green; B, E and H). Single arrows indicate double-labeled neurons. Scale bars = 50 μm. nNOS: Neuronal nitric oxide synthase; TNBS: 2,4,6-trinitrobenzene sulfonic acid; BBG: Brilliant blue G.

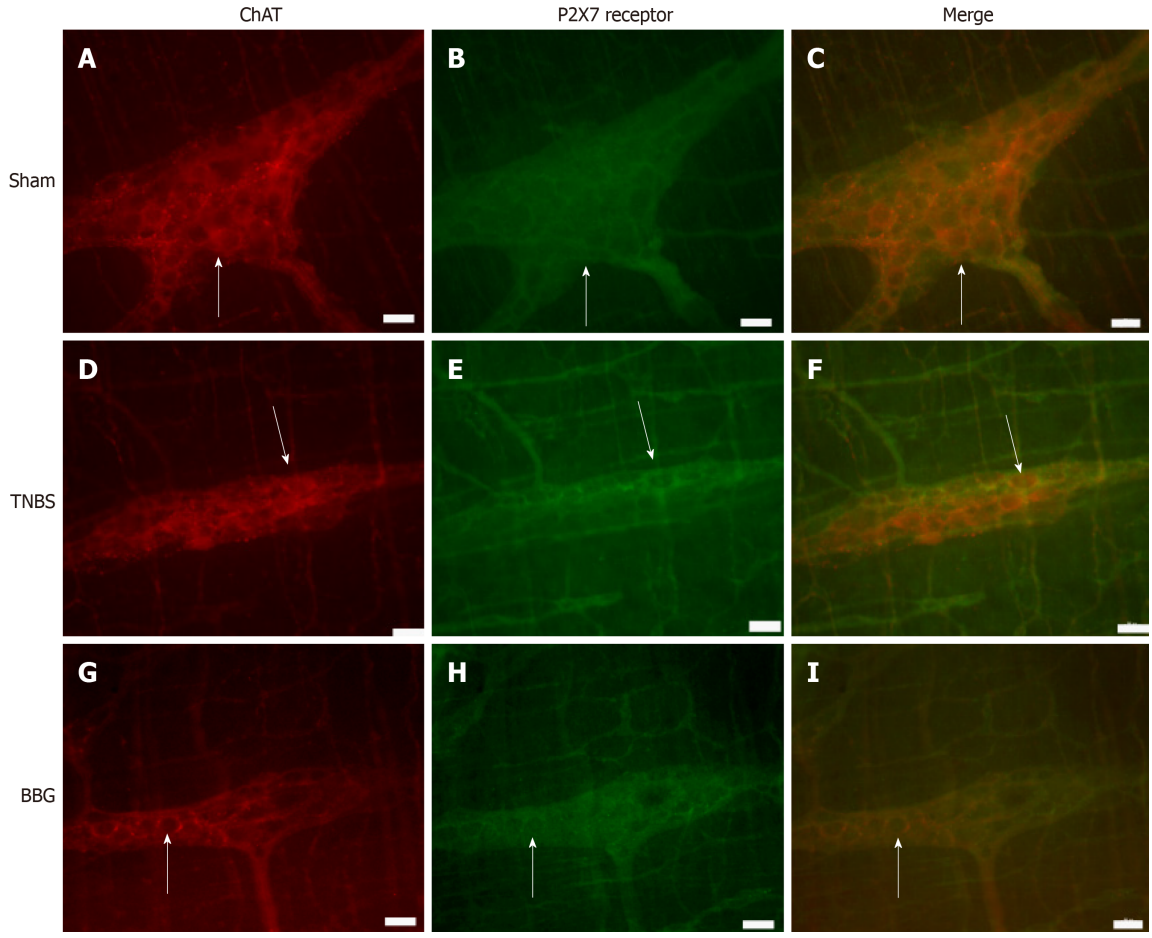

Figure 4 Colocalization of the P2X7 receptor with choline acetyltransferase in neurons of the rat ileum myenteric plexus in the sham, 2,4,6-trinitrobenzene sulfonic acid and brilliant blue G groups. A-C: Sham group; D-F: 2,4,6-trinitrobenzene group; G-I: Brilliant blue G group. Choline acetyltransferase immunoreactivity (red; A, D, and G) colocalized with P2X7 immunoreactivity (green; B, E and H). Single arrows indicate double-labeled neurons. Scale bars = 50 μm. ChAT: Choline acetyltransferase; TNBS: 2,4,6-trinitrobenzene sulfonic acid; BBG: Brilliant blue G.

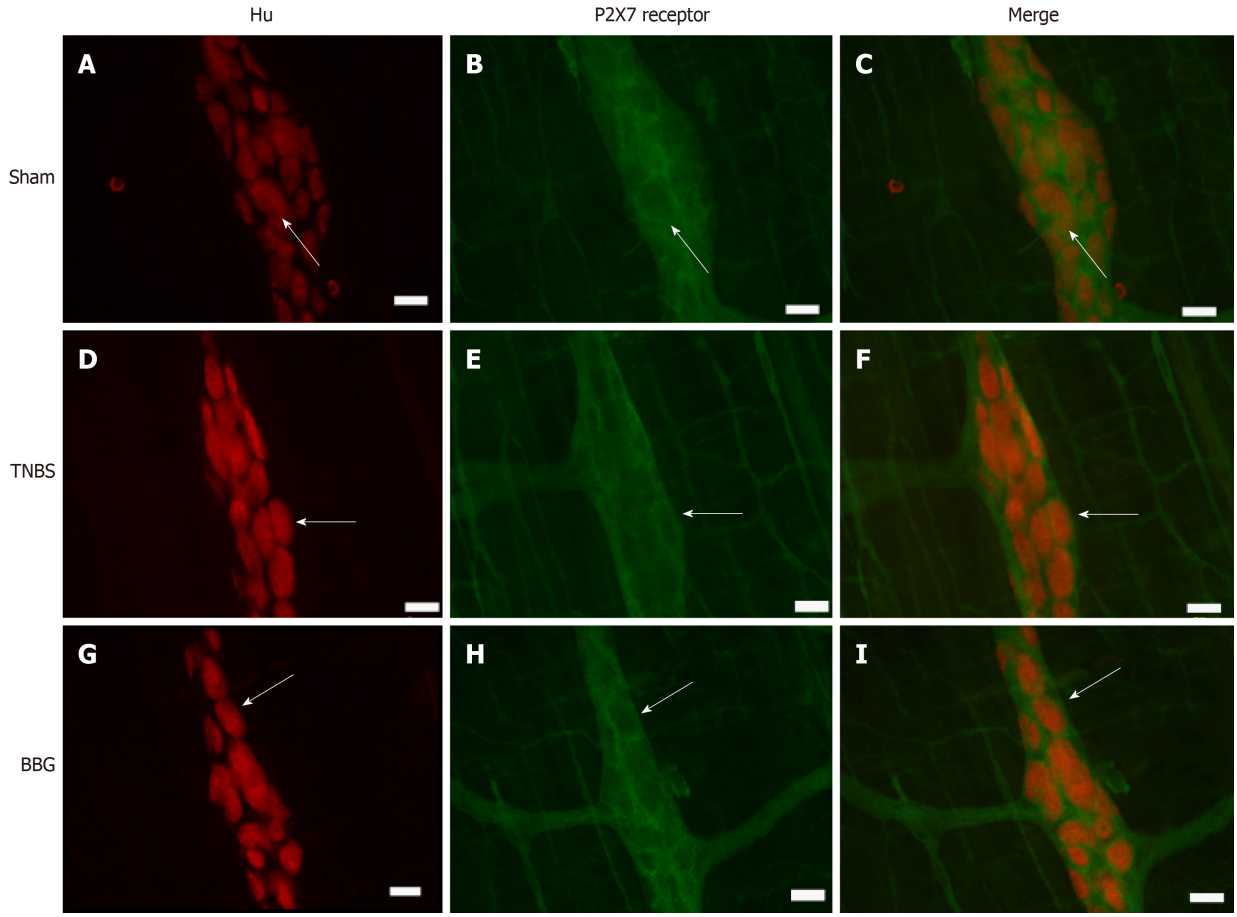

Figure 5 Colocalization of the P2X7 receptor with HuC/D in neurons of the rat ileum myenteric plexus in the sham, 2,4,6-trinitrobenzene sulfonic acid and brilliant blue G groups. A-C: Sham group; D-F: 2,4,6-trinitrobenzene group; G-I: Brilliant blue G group. HuC/D immunoreactivity (red; A, D, and G) colocalized with P2X7 immunoreactivity (green; B, E and H). Single arrows indicate double-labeled neurons. Scale bars = 50 μm. TNBS: 2,4,6-trinitrobenzene sulfonic acid; BBG: Brilliant blue G.

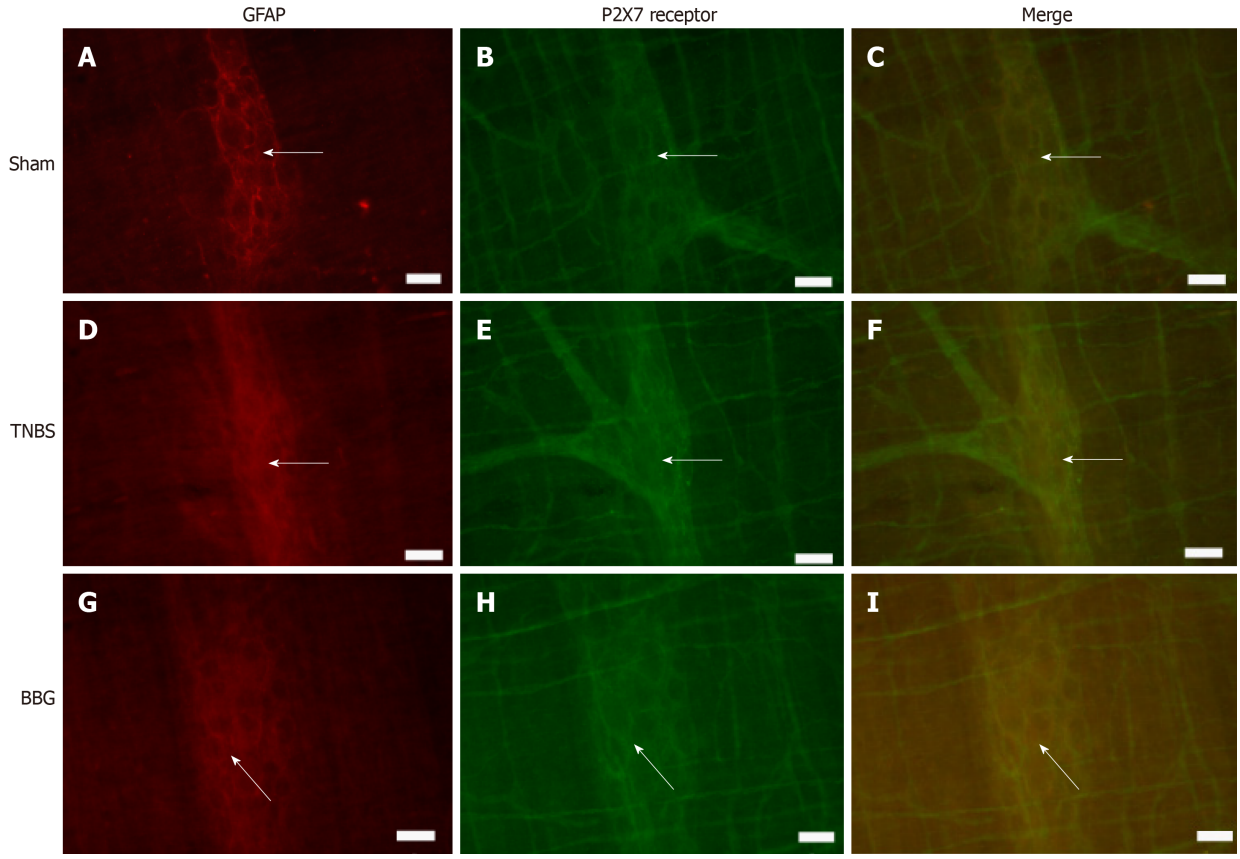

Figure 6 Colocalization of the P2X7 receptor with glial fibrillary acidic protein in the rat ileum myenteric plexus in the sham, 2,4,6-trinitrobenzene sulfonic acid and brilliant blue G groups. A-C: Sham group; D-F: 2,4,6-trinitrobenzene group; G-I: Brilliant blue G group. GFAP immunoreactivity (red; A, D, and G) colocalized with P2X7 immunoreactivity (green; B, E and H). Single arrows indicate double-labeled enteric glial cells. Scale bars = 50 μm. GFAP: Glial fibrillary acidic protein; TNBS: 2,4,6-trinitrobenzene sulfonic acid; BBG: Brilliant blue G.

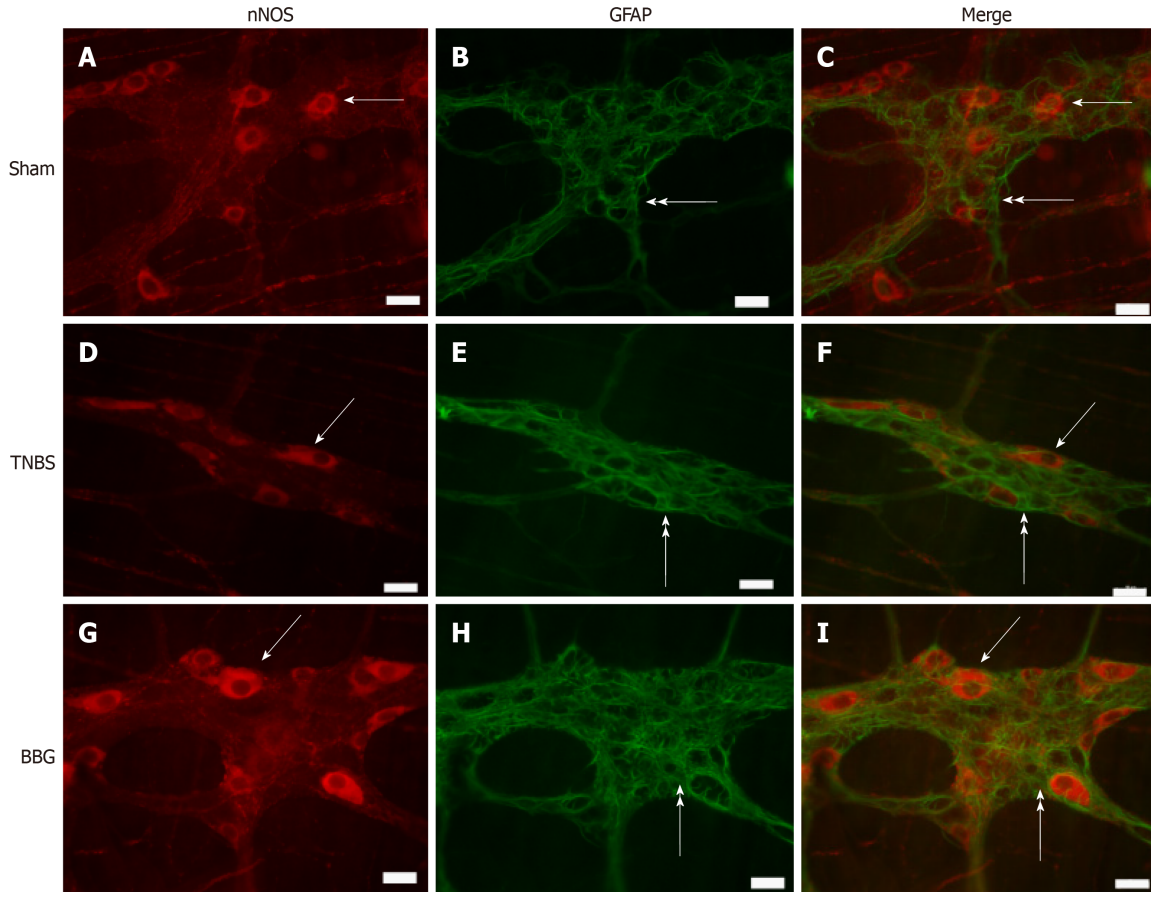

Figure 7 Double labeling of neuronal nitric oxide synthase and glial fibrillary acidic protein in the rat ileum myenteric plexus in the sham, 2,4,6-trinitrobenzene sulfonic acid and brilliant blue G groups. A-C: Sham group; D-F: 2,4,6-trinitrobenzene group; G-I: Brilliant blue G group. Neuronal nitric oxide synthase immunoreactivity (red; A, D, and G) did not colocalize with glial fibrillary acidic protein immunoreactivity (green; B, E and H). Single arrows indicate labeling of neuronal nitric oxide synthase-positive neurons, and double arrows indicate enteric glial cell positivity. Scale bars = 50 μm. nNOS: Neuronal nitric oxide synthase; GFAP: Glial fibrillary acidic protein; TNBS: 2,4,6-trinitrobenzene sulfonic acid; BBG: Brilliant blue G.

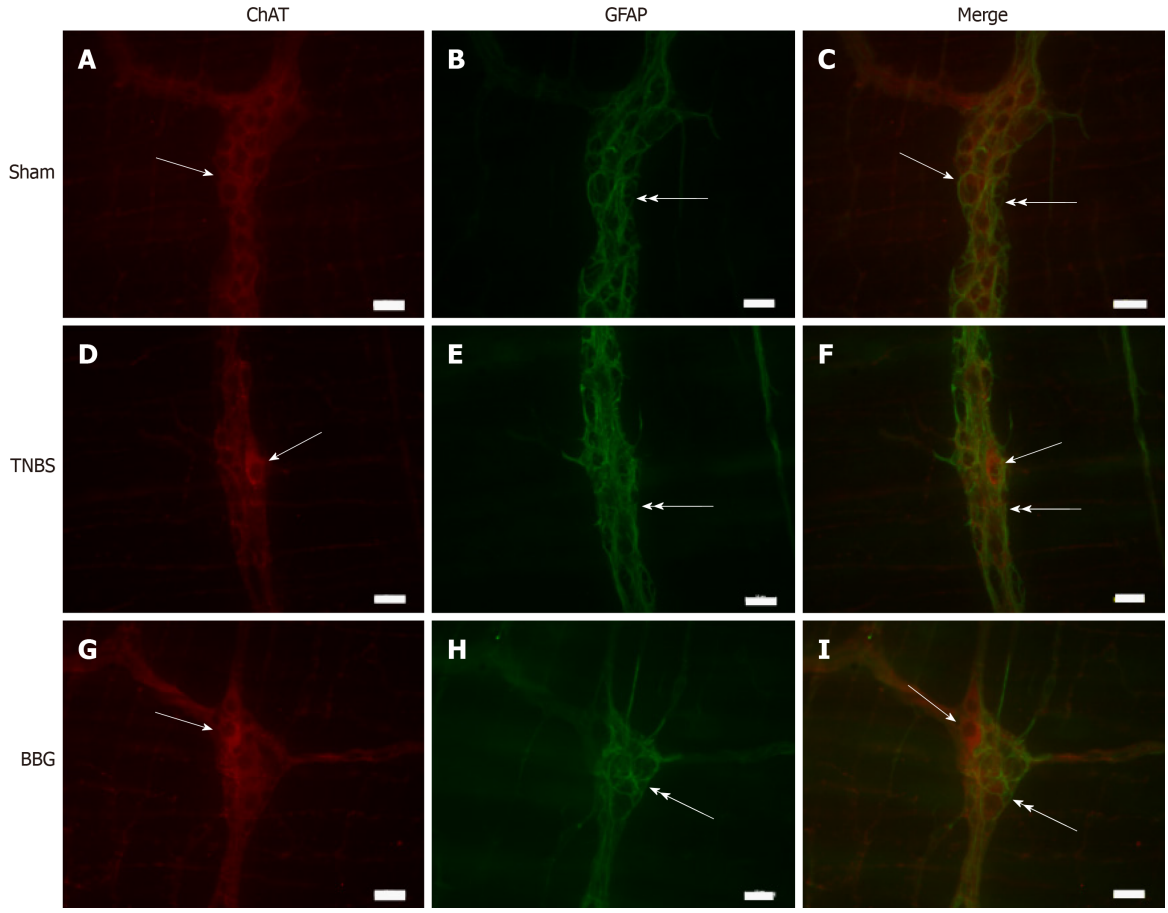

Figure 8 Double labeling of choline acetyltransferase with glial fibrillary acidic protein in the rat ileum myenteric plexus in the sham, 2,4,6-trinitrobenzene sulfonic acid and brilliant blue G groups. A-C: Sham group; D-F: 2,4,6-trinitrobenzene group; G-I: Brilliant blue G group. Choline acetyltransferase immunoreactivity (red; A, D, and G) did not colocalize with glial fibrillary acidic protein immunoreactivity (green; B, E and H). Single arrows indicate choline acetyltransferase-positive neurons, and double arrows indicate enteric glial cell positivity. Scale bars = 50 μm. ChAT: Choline acetyltransferase; GFAP: Glial fibrillary acidic protein; TNBS: 2,4,6-trinitrobenzene sulfonic acid; BBG: Brilliant blue G.

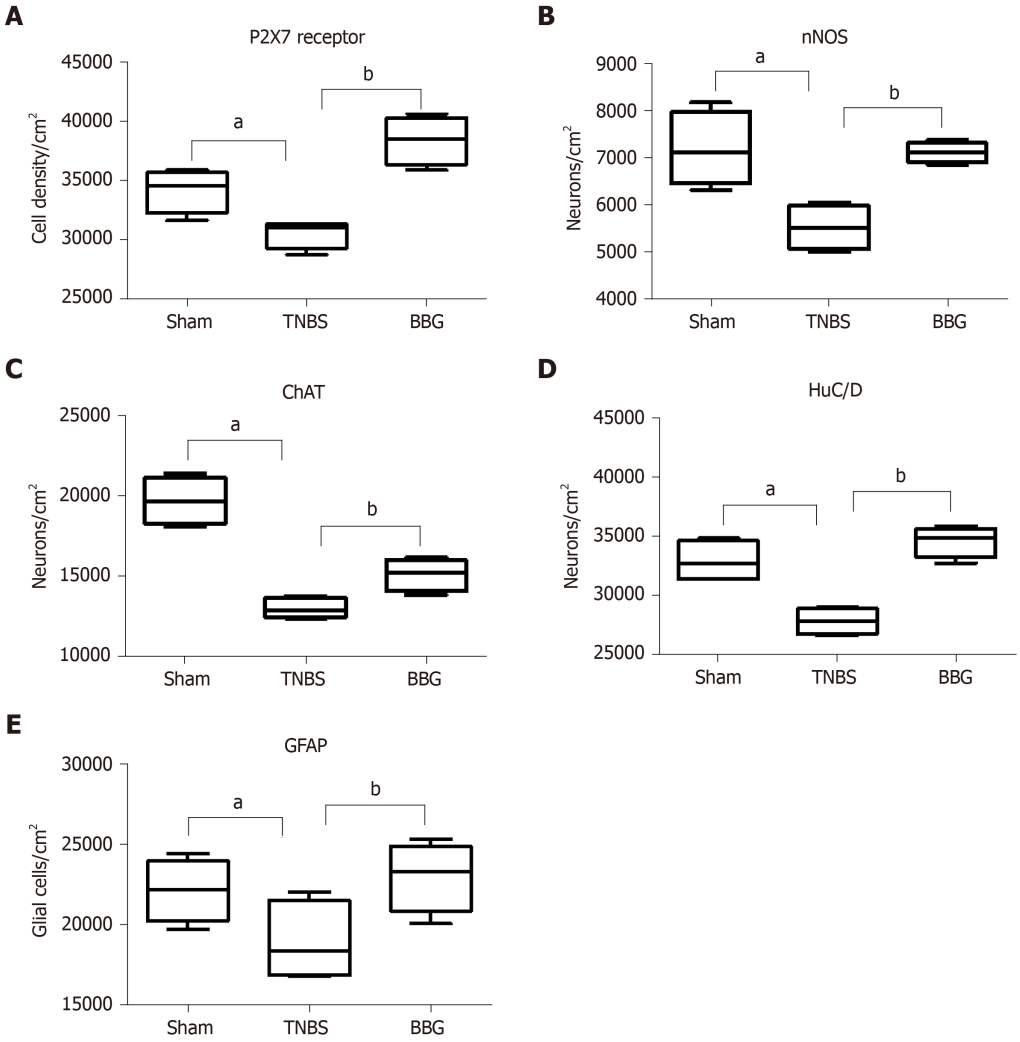

Figure 9 Density of neurons expression in neurons of the rat ileum myenteric plexus in the sham, 2,4,6-trinitrobenzene sulfonic acid and brilliant blue G groups. A: P2X7 receptor; B: Neuronal nitric oxide synthase; C: Choline acetyltransferase; D: HuC/D; E: Glial fibrillary acidic protein. Counts were made in 40 representative fields for each antigen from each animal from the sham (n = 5), 2,4,6-trinitrobenzene sulfonic acid (TNBS) (n = 5) and brilliant blue G (BBG) groups (n = 5). Data were compared using analysis of variance and Tukey's test for multiple comparisons as appropriate. $P < 0.05$ was considered statistically significant. $^{a}P < 0.05$, comparing the TNBS group and sham group; $^{b}P < 0.05$, comparing the BBG group and TNBS group. The data are expressed as mean ± SE. nNOS: Neuronal nitric oxide synthase; ChAT: Choline acetyltransferase; GFAP: Glial fibrillary acidic protein; TNBS: 2,4,6-trinitrobenzene sulfonic acid; BBG: Brilliant blue G.

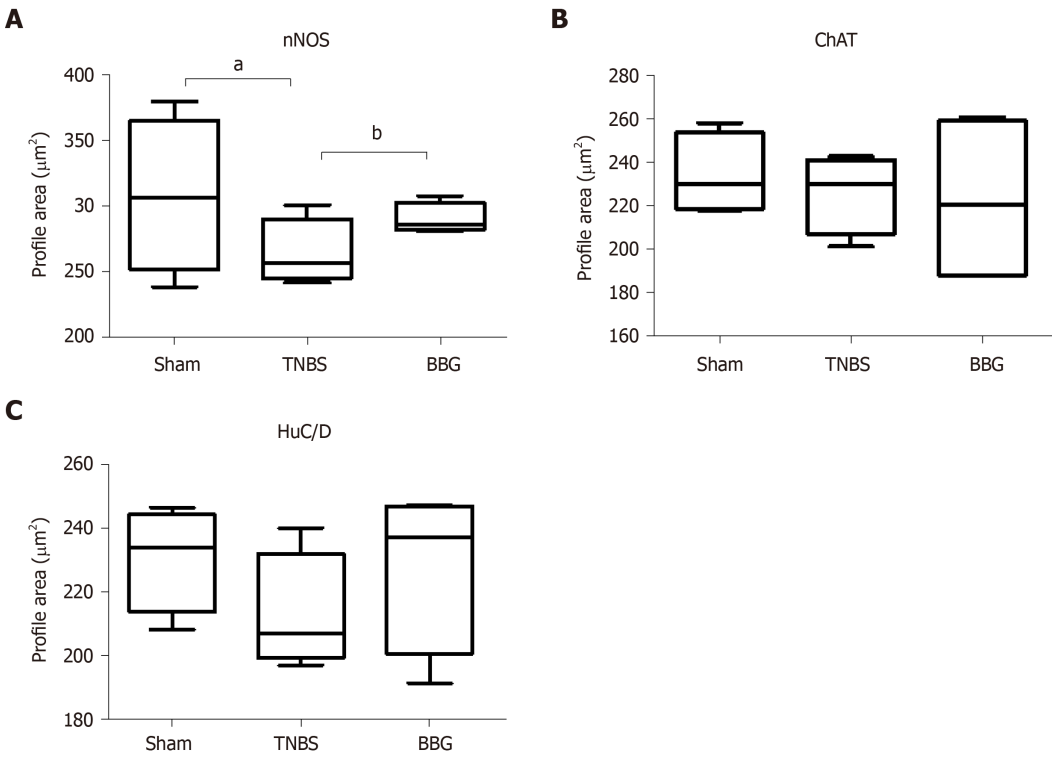

Figure 10 Cell body profile areas of neurons immunoreactive in neurons of the rat ileum myenteric plexus in the sham, 2,4,6-trinitrobenzene sulfonic acid and brilliant blue G groups. A: Neuronal nitric oxide synthase (nNOS); B: Choline acetyltransferase (ChAT); C: HuC/D. The cell perikaryal profile areas (μm^2) of 100 neurons from each animal were obtained in the sham (n = 5), 2,4,6-trinitrobenzene sulfonic acid (TNBS) (n = 5) and Brilliant blue G (BBG) groups (n = 5). A total of 500 cell profile areas were analyzed for each group. Data were compared using analysis of variance and Tukey's test for multiple comparisons as appropriate. P < 0.05 was considered statistically significant. [a]P < 0.05, comparing the TNBS group and sham group; [b]P < 0.05, comparing the BBG group and TNBS group. The data are expressed as mean ± SE. nNOS: Neuronal nitric oxide synthase; ChAT: Choline acetyltransferase; TNBS: 2,4,6-trinitrobenzene sulfonic acid; BBG: Brilliant blue G.

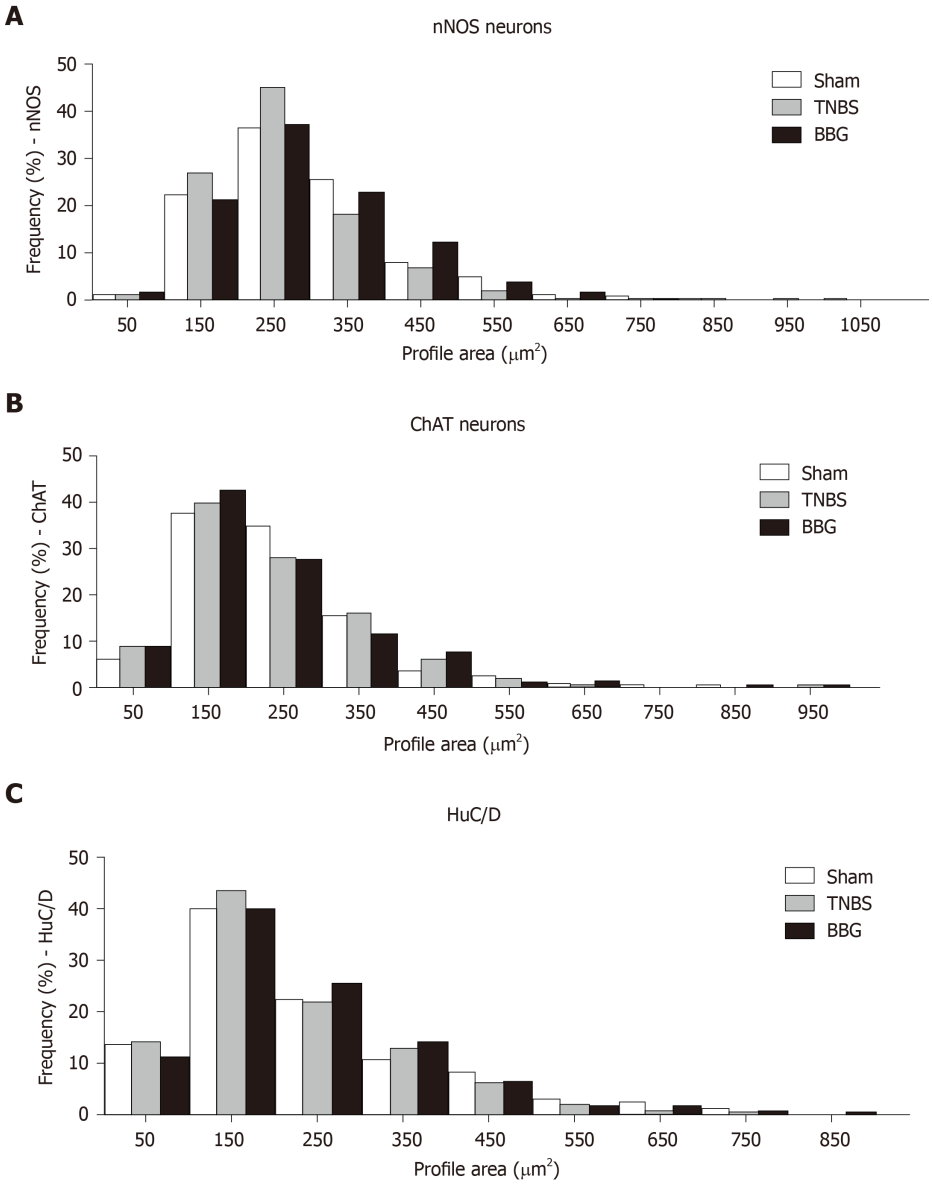

Figure 11 Frequency distribution in cell profiles of neuronal immunoreactivity of neurons among neurons of the rat ileum myenteric plexus in the sham, 2,4,6-trinitrobenzene sulfonic acid and brilliant blue G groups. A: Neuronal nitric oxide synthase (nNOS); B: Choline acetyltransferase (ChAT); C: HuC/D. The size of nNOS-immunoreactive neurons ranged from 50-1050 μm^2. The size of ChAT-immunoreactive neurons ranged from 50-950 μm^2. The size of HuC/D neurons ranged from 50-850 μm^2. The cell perikaryal profile areas of 100 neurons positive for nNOS, ChAT and HuC/D cells from each animal were obtained in the sham (n = 5), 2,4,6-trinitrobenzene sulfonic acid (n = 5) and brilliant blue G groups (n = 5). nNOS: Neuronal nitric oxide synthase; ChAT: Choline acetyltransferase; TNBS: 2,4,6-trinitrobenzene sulfonic acid; BBG: Brilliant blue G.

ARTICLE HIGHLIGHTS

Research background

The enteric nervous system performs functions in gastrointestinal tract such as motility, control of gastric acid secretion, regulation of fluid movement through the epithelium. This system has two ganglionic plexuses, the myenteric plexus and the submucosal plexus. Inflammatory bowel diseases (IBDs) are disorders that include ulcerative colitis and Crohn's disease. In experimental ulcerative colitis, there are changes in enteric neurons. The P2X7 receptor has been described in the ENS.

Research motivation

Studies have demonstrated that P2X7 antagonist, brilliant blue G (BBG) recovers neurons following injuries.

Research objectives

The topics of this work were to analyze the effects of experimental ulcerative colitis in enteric neurons and enteric glial cells in the ileum in animals treated with P2X7 antagonist (BBG).

Research methods
The rats were anesthetized with a mixture of xylazine (20 mg/kg) and ketamine (100 mg/kg) administered subcutaneously. Inflammation was induced through the intrarectal insertion of a polypropylene 8 cm cannula. 2,4,6-trinitrobenzene sulfonic acid (TNBS, Sigma, Saint Louis, United States) was injected at a dose of 30 mg/kg in 600 µL of 30% ethanol in the colon lumen (n = 5). Sham animals (n = 5) were injected with vehicle. BBG (50 mg/kg, Sigma Aldrich, United Kingdom, n = 5) or saline was injected 1 h following TNBS injection (n = 5). The survival time after colitis induction was 24 h. For immunohistochemistry, fresh segments of the ileum were dissected after fixed. Double labeling has been done of P2X7 receptor with neuronal nitric oxide synthase (nNOS), choline acetyltransferase (ChAT), and HuC/D (a pan-neuronal marker) and enteric glial cells immunoreactive for glial fibrillary acidic protein (GFAP). The stained tissue specimens were examined using a Nikon 80i fluorescent and Confocal microscope. The counting of the neurons per area and glial cell were done in fluorescent microscope.

Research results
The numbers of nNOS-, ChAT-, HuC/D- immunoreactive (ir) neurons and GFAP-ir glial cells were decreased in the TNBS group and recovered in the BBG group. The neuronal profile area (μm^2) demonstrated that nNOS-ir neurons decreased in the TNBS group and recovered in the BBG group. There were no differences in the profile areas of ChAT- and HuC/D-ir neurons. Our data conclude that ileum myenteric neurons and glial cells were affected by ulcerative colitis and that treatment with BBG had a neuroprotective effect. Thus, these results demonstrate that the P2X7 receptor may be an important target in therapeutic strategies.

Research conclusions
Ileum myenteric neurons and glial cells were affected by experimental ulcerative colitis and that treatment with P2X7 receptor antagonist, BBG had a neuroprotective effect. The results demonstrate that the P2X7 receptor may be an important target in therapeutic strategies. P2X7 receptor may be a possible therapeutic target in the treatment of the effects of experimental ulcerative colitis Ileum myenteric neurons and glial cells were affected by experimental ulcerative colitis and treatment with BBG may recover enteric neurons. P2X7 receptor may be a possible therapeutic target in the treatment of the experimental ulcerative colitis. Injection of BBG (50 mg/kg, Sigma Aldrich, United Kingdom) for experimental ulcerative colitis and effects in the distal ileum. Inflammation was induced through the intrarectal insertion of a polypropylene 8 cm cannula. 2,4,6-trinitrobenzene sulfonic acid (TNBS, Sigma, Saint Louis, United States) was injected at a dose of 30 mg/kg in 600 µL of 30% ethanol in the colon lumen. There was affected the distal ileum. Additionally, injection of BBG recover enteric neurons distal ileum. Studies show that BBG is a P2X7 antagonist, and its low toxicity and high selectivity make this compound an ideal candidate to block the adverse effects of P2X7 receptor activation. BBG treatment was shown to be effective in the recovery of ileum myenteric neurons, thus demonstrating that the P2X7 receptor may be a possible therapeutic target in the treatment of the effects of experimental ulcerative colitis.

Research perspectives
Study of effects of the experimental ulcerative colitis in the ileum and may use of the P2X7 receptor for therapeutic target. Additionally, study effects of BBG in the distal colon following experimental ulcerative colitis. The direction of the future research will be study effects of the experimental ulcerative colitis of myenteric neurons in the P2X7 receptor-deficient animals. The best method will be use P2X7 receptor-deficient animals.

REFERENCES

1 **Furness JB**. The enteric nervous system and neurogastroenterology. *Nat Rev Gastroenterol Hepatol* 2012; **9**: 286-294 [PMID: 22392290 DOI: 10.1038/nrgastro.2012.32]
2 **Furness JB**. The Enteric Nervous System. MA: Blackwell Publishing, 2006
3 **Gabella G**. Neuron size and number in the myenteric plexus of the newborn and adult rat. *J Anat* 1971; **109**: 81-95 [PMID: 5556678]
4 **Bassotti G**, Villanacci V, Fisogni S, Rossi E, Baronio P, Clerici C, Maurer CA, Cathomas G, Antonelli E. Enteric glial cells and their role in gastrointestinal motor abnormalities: introducing the neuro-gliopathies. *World J Gastroenterol* 2007; **13**: 4035-4041 [PMID: 17696219 DOI: 10.3748/wjg.v13.i30.4035]
5 **Kawada M**, Arihiro A, Mizoguchi E. Insights from advances in research of chemically induced experimental models of human inflammatory bowel disease. *World J Gastroenterol* 2007; **13**: 5581-5593 [PMID: 17948932 DOI: 10.3748/wjg.v13.i42.5581]
6 **da Silva MV**, Marosti AR, Mendes CE, Palombit K, Castelucci P. Submucosal neurons and enteric glial cells expressing the P2X7 receptor in rat experimental colitis. *Acta Histochem* 2017; **119**: 481-494 [PMID: 28501138 DOI: 10.1016/j.acthis.2017.05.001]
7 **da Silva MV**, Marosti AR, Mendes CE, Palombit K, Castelucci P. Differential effects of experimental ulcerative colitis on P2X7 receptor expression in enteric neurons. *Histochem Cell Biol* 2015; **143**: 171-184 [PMID: 25201348 DOI: 10.1007/s00418-014-1270-6]
8 **Linden DR**, Couvrette JM, Ciolino A, McQuoid C, Blaszyk H, Sharkey KA, Mawe GM. Indiscriminate loss of myenteric neurones in the TNBS-inflamed guinea-pig distal colon. *Neurogastroenterol Motil* 2005; **17**: 751-760 [PMID: 16185315 DOI: 10.1111/j.1365-2982.2005.00703.x]
9 **Neunlist M**, Aubert P, Toquet C, Oreshkova T, Barouk J, Lehur PA, Schemann M, Galmiche JP. Changes in chemical coding of myenteric neurones in ulcerative colitis. *Gut* 2003; **52**: 84-90 [PMID: 12477766 DOI: 10.1136/gut.52.1.84]
10 **Poli E**, Lazzaretti M, Grandi D, Pozzoli C, Coruzzi G. Morphological and functional alterations of the

myenteric plexus in rats with TNBS-induced colitis. *Neurochem Res* 2001; **26**: 1085-1093 [PMID: 11699935 DOI: 10.1023/a:1012313424144]
11 **McCready FJ**, Bargen JA. Involvement of the ileum in chronic ulcerative colitis. *N Engl J Med* 1949; **240**: 119-127 [PMID: 18108072 DOI: 10.1056/nejm194901272400401]
12 **Antonioli L**, Blandizzi C, Giron MC. Enteric purinergic signaling: Shaping the "brain in the gut". *Neuropharmacology* 2015; **95**: 477-478 [PMID: 25981956 DOI: 10.1016/j.neuropharm.2015.04.021]
13 **Antonioli L**, Colucci R, Pellegrini C, Giustarini G, Tuccori M, Blandizzi C, Fornai M. The role of purinergic pathways in the pathophysiology of gut diseases: pharmacological modulation and potential therapeutic applications. *Pharmacol Ther* 2013; **139**: 157-188 [PMID: 23588157 DOI: 10.1016/j.pharmthera.2013.04.002]
14 **Antonioli L**, Giron MC, Colucci R, Pellegrini C, Sacco D, Caputi V, Orso G, Tuccori M, Scarpignato C, Blandizzi C, Fornai M. Involvement of the P2X7 purinergic receptor in colonic motor dysfunction associated with bowel inflammation in rats. *PLoS One* 2014; **9**: e116253 [PMID: 25549098 DOI: 10.1371/journal.pone.0116253]
15 **Burnstock G**. Purinergic signalling and disorders of the central nervous system. *Nat Rev Drug Discov* 2008; **7**: 575-590 [PMID: 18591979 DOI: 10.1038/nrd2605]
16 **Burnstock G**, Straub RW, Bolis L. A basis for distinguishing two types of purinergic receptor. In: Straub RW, Bolis L. Cell membrane receptors for drugs and hormones: a multidiciplinary aproach. Straub RW, Bolis L. New York: Raven Press, 1978: 107-118
17 **Burnstock G**. The journey to establish purinergic signalling in the gut. *Neurogastroenterol Motil* 2008; **20** Suppl 1: 8-19 [PMID: 18402638 DOI: 10.1111/j.1365-2982.2008.01107.x]
18 **North RA**, Surprenant A. Pharmacology of cloned P2X receptors. *Annu Rev Pharmacol Toxicol* 2000; **40**: 563-580 [PMID: 10836147 DOI: 10.1146/annurev.pharmtox.40.1.563]
19 **Abbracchio MP**, Burnstock G, Verkhratsky A, Zimmermann H. Purinergic signalling in the nervous system: an overview. *Trends Neurosci* 2009; **32**: 19-29 [PMID: 19008000 DOI: 10.1016/j.tins.2008.10.001]
20 **Di Virgilio F**, Chiozzi P, Falzoni S, Ferrari D, Sanz JM, Venketaraman V, Baricordi OR. Cytolytic P2X purinoceptors. *Cell Death Differ* 1998; **5**: 191-199 [PMID: 10200464 DOI: 10.1038/sj.cdd.4400341]
21 **Volonté C**, D'Ambrosi N. Membrane compartments and purinergic signalling: the purinome, a complex interplay among ligands, degrading enzymes, receptors and transporters. *FEBS J* 2009; **276**: 318-329 [PMID: 19076212 DOI: 10.1111/j.1742-4658.2008.06793.x]
22 **Hu HZ**, Gao N, Lin Z, Gao C, Liu S, Ren J, Xia Y, Wood JD. P2X(7) receptors in the enteric nervous system of guinea-pig small intestine. *J Comp Neurol* 2001; **440**: 299-310 [PMID: 11745625 DOI: 10.1002/cne.1387]
23 **Palombit K**, Mendes CE, Tavares-de-Lima W, Silveira MP, Castelucci P. Effects of ischemia and reperfusion on subpopulations of rat enteric neurons expressing the P2X7 receptor. *Dig Dis Sci* 2013; **58**: 3429-3439 [PMID: 23990036 DOI: 10.1007/s10620-013-2847-y]
24 **Remy M**, Thaler S, Schumann RG, May CA, Fiedorowicz M, Schuettauf F, Grüterich M, Priglinger SG, Nentwich MM, Kampik A, Haritoglou C. An in vivo evaluation of Brilliant Blue G in animals and humans. *Br J Ophthalmol* 2008; **92**: 1142-1147 [PMID: 18653608 DOI: 10.1136/bjo.2008.138164]
25 **Burnstock G**, Volonté C. Pharmacology and therapeutic activity of purinergic drugs for disorders of the nervous system. *CNS Neurol Disord Drug Targets* 2012; **11**: 649-651 [PMID: 22963433 DOI: 10.2174/18715271280358113 7]
26 **Jiang LH**, Mackenzie AB, North RA, Surprenant A. Brilliant blue G selectively blocks ATP-gated rat P2X(7) receptors. *Mol Pharmacol* 2000; **58**: 82-88 [PMID: 10860929 DOI: 10.1124/mol.58.1.82]
27 **Figliuolo VR**, Savio LEB, Safya H, Nanini H, Bernardazzi C, Abalo A, de Souza HSP, Kanellopoulos J, Bobé P, Coutinho CMLM, Coutinho-Silva R. P2X7 receptor promotes intestinal inflammation in chemically induced colitis and triggers death of mucosal regulatory T cells. *Biochim Biophys Acta Mol Basis Dis* 2017; **1863**: 1183-1194 [PMID: 28286160 DOI: 10.1016/j.bbadis.2017.03.004]
28 **Peng W**, Cotrina ML, Han X, Yu H, Bekar L, Blum L, Takano T, Tian GF, Goldman SA, Nedergaard M. Systemic administration of an antagonist of the ATP-sensitive receptor P2X7 improves recovery after spinal cord injury. *Proc Natl Acad Sci USA* 2009; **106**: 12489-12493 [PMID: 19666625 DOI: 10.1073/pnas.0902531106]
29 **Palombit K**, Mendes CE, Tavares-de-Lima W, Barreto-Chaves ML, Castelucci P. Blockage of the P2X7 Receptor Attenuates Harmful Changes Produced by Ischemia and Reperfusion in the Myenteric Plexus. *Dig Dis Sci* 2019; **64**: 1815-1829 [PMID: 30734238 DOI: 10.1007/s10620-019-05496-8]
30 **Bell CJ**, Gall DG, Wallace JL. Disruption of colonic electrolyte transport in experimental colitis. *Am J Physiol* 1995; **268**: G622-G630 [PMID: 7733288 DOI: 10.1152/ajpgi.1995.268.4.G622]
31 **Erdogan B**, Isiksoy S, Dundar E, Pasaoglu O, Bal C. The effects of sodium phosphate and polyethylene glycol-electrolyte bowel preparation solutions on 2,4,6-trinitrobenzenesulfonic acid-induced colitis in the rat. *Exp Toxicol Pathol* 2003; **55**: 213-220 [PMID: 14620544 DOI: 10.1078/0940-2993-00318]
32 **Fabia R**, Ar'Rajab A, Johansson ML, Willén R, Andersson R, Molin G, Bengmark S. The effect of exogenous administration of Lactobacillus reuteri R2LC and oat fiber on acetic acid-induced colitis in the rat. *Scand J Gastroenterol* 1993; **28**: 155-162 [PMID: 8382837 DOI: 10.3109/00365529309096063]
33 **Cooper HS**, Murthy SN, Shah RS, Sedergran DJ. Clinicopathologic study of dextran sulfate sodium experimental murine colitis. *Lab Invest* 1993; **69**: 238-249 [PMID: 8350599]
34 **Nooh HZ**, Nour-Eldien NM. The dual anti-inflammatory and antioxidant activities of natural honey promote cell proliferation and neural regeneration in a rat model of colitis. *Acta Histochem* 2016; **118**: 588-595 [PMID: 27378376 DOI: 10.1016/j.acthis.2016.06.006]
35 **Jacobson K**, McHugh K, Collins SM. The mechanism of altered neural function in a rat model of acute colitis. *Gastroenterology* 1997; **112**: 156-162 [PMID: 8978354 DOI: 10.1016/s0016-5085(97)70230-0]
36 **Elson CO**, Sartor RB, Targan SR, Sandborn WJ. Challenges in IBD Research: updating the scientific agendas. *Inflamm Bowel Dis* 2003; **9**: 137-153 [PMID: 12792219 DOI: 10.1097/00054725-200305000-00001]
37 **Sanovic S**, Lamb DP, Blennerhassett MG. Damage to the enteric nervous system in experimental colitis. *Am J Pathol* 1999; **155**: 1051-1057 [PMID: 10514387 DOI: 10.1016/s0002-9440(10)65207-8]
38 **Boyer L**, Ghoreishi M, Templeman V, Vallance BA, Buchan AM, Jevon G, Jacobson K. Myenteric plexus injury and apoptosis in experimental colitis. *Auton Neurosci* 2005; **117**: 41-53 [PMID: 15620569 DOI: 10.1016/j.autneu.2004.10.006]
39 **Winston JH**, Li Q, Sarna SK. Paradoxical regulation of ChAT and nNOS expression in animal models of Crohn's colitis and ulcerative colitis. *Am J Physiol Gastrointest Liver Physiol* 2013; **305**: G295-G302

[PMID: 23681475 DOI: 10.1152/ajpgi.00052.2013]
40 **Gulbransen BD**, Bashashati M, Hirota SA, Gui X, Roberts JA, MacDonald JA, Muruve DA, McKay DM, Beck PL, Mawe GM, Thompson RJ, Sharkey KA. Activation of neuronal P2X7 receptor-pannexin-1 mediates death of enteric neurons during colitis. *Nat Med* 2012; **18**: 600-604 [PMID: 22426419 DOI: 10.1038/nm.2679]
41 **Franke H**, Krügel U, Illes P. P2 receptors and neuronal injury. *Pflugers Arch* 2006; **452**: 622-644 [PMID: 16645849 DOI: 10.1007/s00424-006-0071-8]
42 **Geboes K**, Collins S. Structural abnormalities of the nervous system in Crohn's disease and ulcerative colitis. *Neurogastroenterol Motil* 1998; **10**: 189-202 [PMID: 9659662 DOI: 10.1046/j.1365-2982.1998.00102.x]
43 **Mihara H**, Boudaka A, Shibasaki K, Yamanaka A, Sugiyama T, Tominaga M. Involvement of TRPV2 activation in intestinal movement through nitric oxide production in mice. *J Neurosci* 2010; **30**: 16536-16544 [PMID: 21147993 DOI: 10.1523/JNEUROSCI.4426-10.2010]
44 **Gulbransen BD**, Sharkey KA. Novel functional roles for enteric glia in the gastrointestinal tract. *Nat Rev Gastroenterol Hepatol* 2012; **9**: 625-632 [PMID: 22890111 DOI: 10.1038/nrgastro.2012.138]
45 **Gulbransen BD**, Christofi FL. Are We Close to Targeting Enteric Glia in Gastrointestinal Diseases and Motility Disorders? *Gastroenterology* 2018; **155**: 245-251 [PMID: 29964042 DOI: 10.1053/j.gastro.2018.06.050]
46 **Hofman P**, Cherfils-Vicini J, Bazin M, Ilie M, Juhel T, Hébuterne X, Gilson E, Schmid-Alliana A, Boyer O, Adriouch S, Vouret-Craviari V. Genetic and pharmacological inactivation of the purinergic P2RX7 receptor dampens inflammation but increases tumor incidence in a mouse model of colitis-associated cancer. *Cancer Res* 2015; **75**: 835-845 [PMID: 25564520 DOI: 10.1158/0008-5472.CAN-14-1778]
47 **Mihara H**, Boudaka A, Tominaga M, Sugiyama T. Transient Receptor Potential Vanilloid 4 Regulation of Adenosine Triphosphate Release by the Adenosine Triphosphate Transporter Vesicular Nucleotide Transporter, a Novel Therapeutic Target for Gastrointestinal Baroreception and Chronic Inflammation. *Digestion* 2020; **101**: 6-11 [PMID: 31770754 DOI: 10.1159/000504021]

Published by Baishideng Publishing Group Inc
7041 Koll Center Parkway, Suite 160, Pleasanton, CA 94566, USA
Telephone: +1-925-3991568
E-mail: bpgoffice@wjgnet.com
Help Desk:https://www.f6publishing.com/helpdesk
https://www.wjgnet.com